Pro Gradu

Vapour phase deposition of dye sensitizer

Sampo Kulju

December 23, 2009

UNIVERSITY OF JYVÄSKYLÄ

DEPARTMENT OF PHYSICS

NANOSCIENCE CENTER

Tiivistelmä

Uusiutuvat energiamuodot ja aurinkosähkö ovat kuuma puheenaihe. Myös tutkimustyö tällä saralla on ollut kiivasta viime vuosikymmeninä ja tuloksena on syntynyt esimerkiksi väriaineherkistetyt aurinkokennot. Nämä aurinkokennot voivat olla halpa ratkaisu tulevaisuuden päästöttömään energiantuotantoon, mutta näissä aurinkokennoissa käytetyt valolle herkät väriaineet voivat antaa myös uusia mahdollisuuksia molekyylielektroniikan saralle ja tuleviin nanomittaluokan sovelluksiin. Väriaineiden laajempi käyttö vaatii kuitenkin uudenlaisten värjäysmetodien kehittämistä. Tässä työssä keskityttiinkin väriainehöyrystimen kehittämiseen ja testaamiseen.

Työn alussa tehdään katsaus väriaineisiin ja käydään läpi höyrystämiseen liittyvää teoriaa, kuten filmin muodostumisnopeutta ja erilaisia kasvumoodeja. Tämän jälkeen tutustutaan väriaineherkistettyihin aurinkokennoihin, niiden toimintamekanismiin ja valmistukseen, jonka jälkeen tarkastellaan kiinteän väriaineen mahdollistamia ratkaisuja ja niiden toimintaperiaatetta.

Seuraavassa luvussa käydään läpi värihöyrystimen kehityskaari sekä nykyinen laitteisto kaaviokuvineen. Samalla esitetään myös suoritetut kalibraatiotoimenpiteet sekä lämpö- että paksuusmittarille, ja kuvataan värin höyrystysprosessi.

Näytteenvalmistus- ja tarvittavat litografiaprosessit käydään läpi eri näytetyypeille ja käytetyt mittausjärjestelyt kytkentäkaavioineen ja laitteistoineen kuvataan.

Absorptiospektrien avulla varmistettiin, että väriaine höyrystyy näytteelle. Kiinteän värin spektriä myös verrattiin nesteeseen liuotettuun väriin. Emissiospektrien mittauksella todennettiin, että väri selviää höyrystysprosessista ja on täten vielä aktiivista. Näytteet osoittivat myös valosähköisiä ominaisuuksia. Värjättyjen näytteiden johtavuus parani, kun niitä valaistiin. Vaikutuksen voimakkuus korreloi näytteen absorptiospektrin kanssa. Myös hystereesisefekti oli huomattavissa: tasajännitepyyhkäisyn (negatiivisesta positiiviseen) tuloksena näytteen vastus kasvoi mikä huomattiin takaisin pyyhkäisyn aikana. Vaikutus kuitenkin pystyttiin tuhoamaan nopeasti tarpeeksi suurella negatiivisella jännitteellä.

Höyrystysmetodi todettiin toimivaksi ratkaisuksi ja täten värjääminen voidaan ottaa osaksi litografiaprosessia. Tämä mahdollistaa väriherkistetyt mikro- ja nanorakenteet jotka omaavat edellä kuvatun kaltaisia valosähköisiä ominaisuuksia.

Projekti tehtiin yhteistyössä Jyväskylän yliopiston professori Jouko Korppi-Tommolan fysikaalisen kemian ryhmän kanssa.

Preface

The work reported in this Pro Gradu has been done between June 2008 and May 2009 at Nanoscience Center at the Department of Physics in the University of Jyväskylä.

I would like to thank my supervisors Senior assistant Konstantin Arutyunov and Dr. Pasi Jalkanen for guidance throughout my thesis project. Furthermore, I'd like to thank all the people who is or has been working in Quantum Nanoelectronics group especially Ms. Terhi Hongisto for teaching and advice related to sample fabrication and e-beam lithography. I'd also like to thank the staff of Nanoscience Center for an inspirational surrounding and for many advice and discussions.

Finally, I would like to thank my family and friends for their support and interest towards this project.

Jyväskylä, December 23, 2009

Sampo Kulju

Contents

Introduction & Summary

Dye-sensitized solar cells (DSSC) have been investigated widely in last two decades and the research work has led to good results. Nowadays DSSCs are relatively efficient, but a problem is the long term stability and manufacturing. These dyes used in DSSCs would also give multiple possibilities to nanoapplications, but the typical sensitization method, soaking in solution, doesn't work with nanofabrication.

However increasing interest towards the molecular engineering has already developed different kind of molecule deposition methods. Anyway, these methods being relatively simple, don't suit mass production and don't allow to control the deposited layer thickness.

The main objective of this thesis was the development a vacuum evaporation method for deposition of dye sensitizer molecules on PMMA-masked metal-oxide structures. This was done in high vacuum conditions where dye was sublimated in heated crucible at temperature range 145-160 °C forming a gaseous jet of molecules from the evaporation chamber into the pumped target chamber. Thickness of the deposited dye layer was controlled by the crystal deposition controller that was calibrated with the AFM. Dye deposition were applied to TiO_2 and FTO based components that showed spectral response according to the dye absorption spectra. Photo-electric properties of these components were also measured. Illumination affected the samples during the AC and DC measurements by reducing their resistance. The effect was found to be wavelength dependent and corresponding to the absorption spectrum of the samples.

The method proved to be usable method for integration of dye sensitizers to conventional lithographical fabrication in order to develop dye based light sensitive micro and nano sized electronics. Research of these new possible structures can give us an information about dye-oxide interactions which could benefit the development of DSSCs. They could also provide knowledge of the spectra of the pure dye without any solvent, quantum effects in dye and maybe even serve as a single photon detector.

This project was done in collaboration with Prof. Jouko Korppi-Tommola's group from the department of Chemistry of the University of Jyväskylä. A confocal microscope was operated by Teemu Ihalainen from the department of Biological and Environmental Science of the University of Jyväskylä

Chapter 1

Theory

1.1 Dyes

Organic dyes are old and easy way to stain textiles and threads, and they have been also used for years in a scientific research. For example, water tracking [1] [2] and cleanness investigations [3] have been done with an aid of fluorescein, and it has been also used in medical checks and treatments [4]. The scientific rise of the dyes came on the early 90's when fluorescein was used in first dye-sensitized solar cell (DSSC) [5]. Since then so called N3 (cis-SCN_2^-(2,2'-bipyridyl-4,4'-dicarboxylate)ruthenium(II)) has replaced fluorescein in DSSCs [6] [7], but it has defended its place in the other areas of nanoscience for instance in molecular electronics [8].

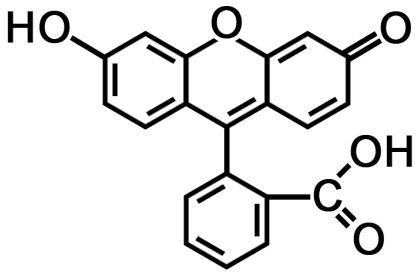

Figure 1.1: Chemical structure of organic dye fluorescein [9].

The base of fluorescein is carbon, as it can be seen from the figure 1.1 where is represented the chemical structure of used fluorescein, neutral p-quinod form [9]. These organic molecules are very good light harvesters; absorbing photons to rise electrons on to a higher energy level. The dyes used in DSSCs are working with relatively high efficiency and for example for N3 dye an electron injection rate to TiO_2 is almost 100% [10] [6].

The absorption spectra of the dyes are in the visible light range, but usually they

have one or two absorption maxima. The absorption spectrum typically depends on the molecule form. Neutral fluorescein species, which were used in our project, have an absorption maximum at 434 nm and a side maximum at 475 nm when they are in a buffer liquid [9]. Usually the peaks are spread and the main peak may screen on the side maximum and this way creates a shoulder on the absorption spectrum.

Dyes also have good adhesion with oxides, like TiO_2 and AlO_X. For example N3 attaches to anatase TiO_2 by carboxylate bonds. This bonding and the fact that the dye's highest occupied molecular orbital (HOMO) is in the band gap of TiO_2 and the lowest unoccupied molecular orbital (LUMO) of the dye is above the conduction band of TiO_2 makes an electron injection possible and this material pair suitable for photoelectric applications [11]. With AlO_X this is not possible because in AlO_X the energy gap is too high for dye to raise electrons to the conduction band.

1.2 Evaporation of molecules

The electronic transport of thin solid materials depends critically on the properties of the interfaces where the charge carriers have to go through [12]. Because of that a doping done by molecular layer on or in the material have been found out to be effective [13]. This has created a need to develop new fabrication methods in the field of the molecular engineering. Evaporation of metals has been used now for decades in micro- and nanofabrication and this method is transfered also to deposit molecules.

Success have been achieved for example in the field of molecular organic light emitting devices (OLEDs), which have been already fabricated by vacuum deposition method [14]. However there is still need to develop a method to deposit organic dyes in vacuum conditions [15] and this way prepare the way for new applications.

1.2.1 Film growth

The film growth during the evaporation process is determined by various different processes. First the evaporated material has to condensate on the substrate surface. The rate of the condensation is described by

$$R = p(2\pi MkT_0)^{-1/2}, \tag{1.1}$$

where p is the vapor pressure, M the molecular weight of the particle, k Boltzmann's constant and T_0 the source temperature. Equation gives a number of particles condensated per m^2 per second.

After a particle has condensated from the vapor phase it may instantly re-evaporate or diffuse on the substrate surface. Diffusion may lead to absorbtion to the special place like a lattice defect, forming a nucleus with an other condensated particle or growing a previously formed film island (Fig. 1.2) [16].

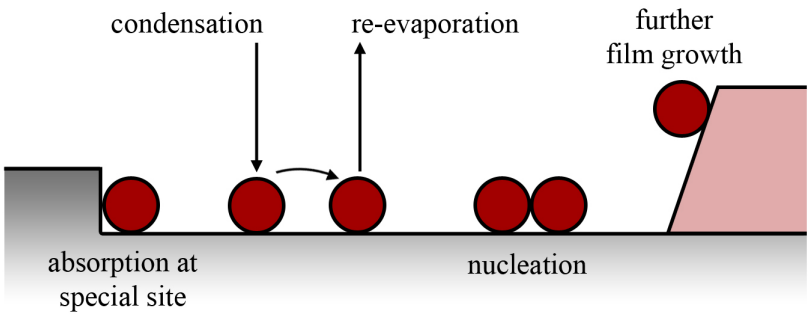

Figure 1.2: Particle processes involved in film growth on a solid substrate [16].

Because of this multiple options after diffusion of the particle, occurs also multiple film growth modes (Fig. 1.3). Three notably different modes exist. In the *layer-by-layer* (Frank-van der Merve, FM) mode the interaction between substrate and evaporated particles is stronger than between neighboring particles. This leads to growing where new layer starts to grow after the last one is fully complete. In the opposite case the interaction between evaporated particles is greater than between substrate and evaporated film. Because of that the particles start to form groups, so called islands, on the surface and this way also gives a name to this growing mode, *island growth* (Vollmer-Weber, VW). Hybrid between these two is the *layer-plus-island* growth mode (Stransky-Krastanov, SK) where after forming monolayer islands, multiple layers are formed on the top if these layers [16].

The growth mode is not a certain material or a substrate dependent constant parameter, but it can vary depending on the evaporation conditions and being a tunable feature.

1.2.2 Methods

Molecules, organic and inorganic, have been deposited through the vapor phase with different ways. One is so called vapor transportation method (VTM), which have been used for whitening the polymer light-emitting diodes with an orange fluorescent dye. In this method samples and a dye were placed in a glass ampoule, system was evacuated to $2 \cdot 10^{-6}$ Pa and the glass tube was shut my melting it. Then whole system was heated to 180°C for 15 hours, to sublimate the dye molecules and disperse them on the sample [17].

Another method relies on the exterior pumping system. It consist of a thin, diameter about 1 mm, polyimide tube which is bent in the middle. The temperature sensor is placed in the other half of the tube and evaporated molecules in the other. Heating wire is coiled around the bent tube and the system is attached to the glass-ceramic connector which can be assembled on the top of the transfer rod and this way install the evaporation system to a UHV chamber. Now a sample can be loaded to the chamber

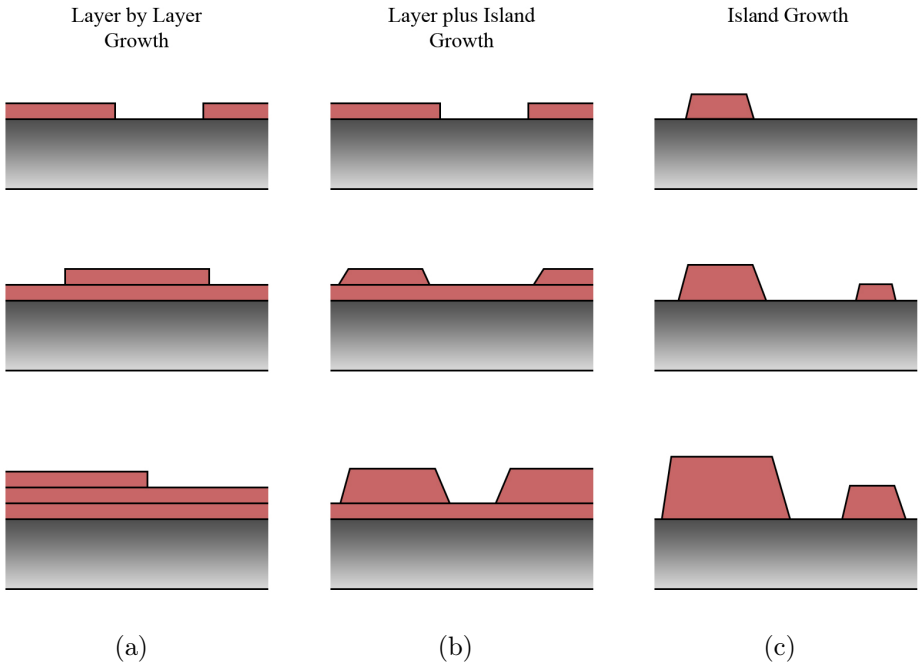

Figure 1.3: Three important growth modes represented in phases where, from top to down, amount of evaporated material is covering less than one monolayer, between one and two monolayers, more than two monolayers. (a) Layer by layer growth. (b) Layer plus island growth. (c) Island growth [16].

and by heating the tube a molecule jet can be attained [18].

Both methods are relatively simple and easy to execute but the main problem is the controlling the amount of molecules, or the layer thickness, deposited by the vapor phase. Neither is suitable for fabrication of large amounts. Therefore more sophisticated methods are needed.

1.3 Applications

To understand the major flaws and strong sides of the both: a solid state dye application, sensitized with evaporated dye, and traditional dye sensitized application with electrolyte, for example DSSC, the basic configuration and principle of the both should be described.

1.3.1 Dye-sensitized solar cell (DSSC)

Fabrication

The fabrication of DSSCs has not changed much since the early days of the application. The fabrication is a relatively simple and straightforward procedure. First a conductive

glass sheet, for example FTO-glass (fluorine-tin-oxide) is covered with TiO_2 layer made from paste containing anatase TiO_2 nanoparticles whose diameter is usually about 10 nm. The nanoparticles are used in order to achieve a large surface area and this way effective dye sensitization. The most simple method for fabricating the layer is to spread paste through a hole made in a scotch tape and flatten it, for example with a glass rod or a surgical knife. With this style the thickness of the TiO_2 layer will be about 1 µm. After, that layer is dried in air for couple of hours and sintered at higher temperature, 350-400 °C, to obtain a transparent layer [19].

Sensitation of the cell is made by several hours soaking in the solution containing dye molecules and solvent, usually dry ethanol. After the dye has absorbed on the surface of the TiO_2 nanoparticle network the sample is dried with a gas flow. Now the cell is ready for storing in dry ethanol or it can be used right away by wetting it with a redox electrolyte and placing a glass sheet with sputtered Pt film on it on the top of the cell. This way a sandwich structured cell is formed and the Pt-glass sheet is working on a mirror and on a counter electrode. [10] The basic structure of DSSC is showed in figure 1.4.

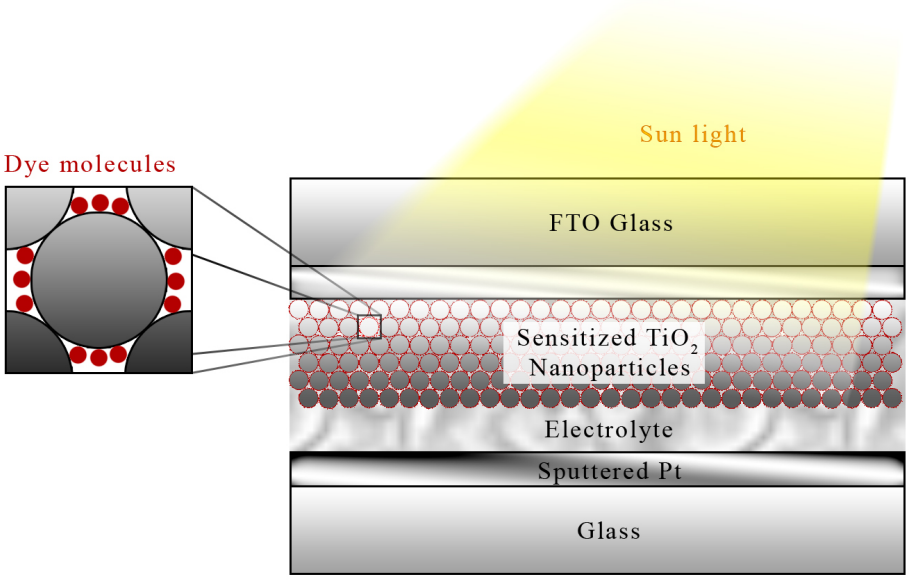

Figure 1.4: The basic structure of DSSC.

Operation under illumination

The principle of a DSSC is relying on the couple of key processes represented in figure 1.5. First step is, of course, a photon absorption which raises an electron in a dye molecule to a higher energy state. This is showed in figure 1.6 illustrating the energy spectrum of a hypothetical DSSC. When the electron is excited from HOMO to LUMO

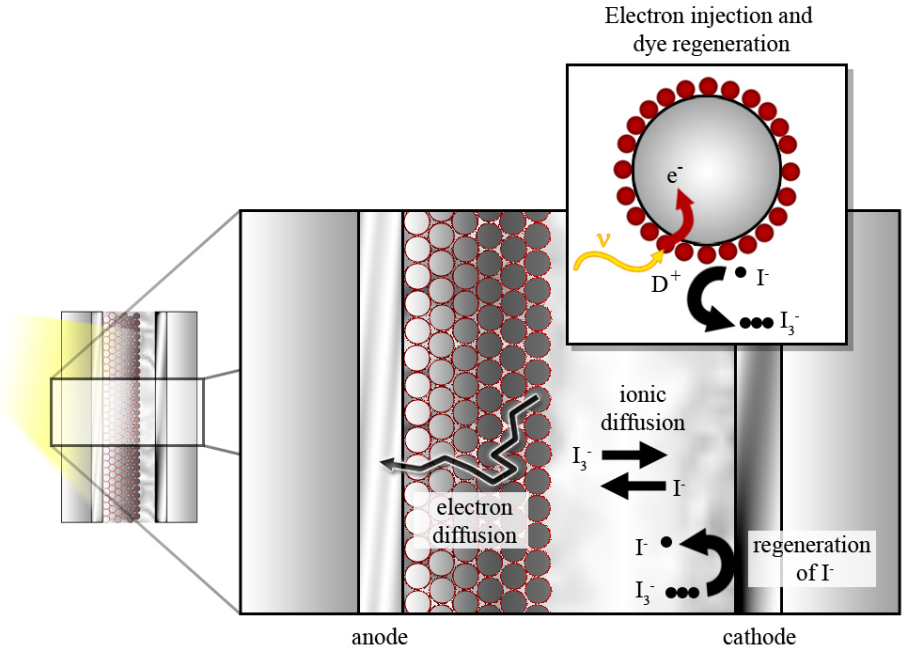

Figure 1.5: Key processes of energy harvesting in a DSSC.

its energy is above the bottom of the conduction band of TiO_2. Now the electron has possibility to go into TiO_2 [20].

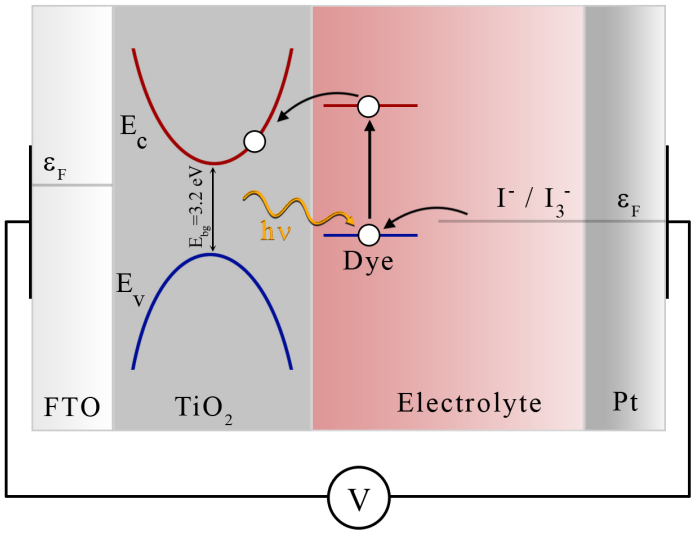

Figure 1.6: Energy spectrum in DSSC.

When excited the electron has two possibilities. There might be a back recombination, but this case, where the electron goes back to dye, is very improbable. More

probable option is the recombination with electrolyte and the hole carriers, triiodides, and this process requires that the electron is in the tunneling distance from the triiodide. However, the hole carriers have negative absolute charge which repulses the electron, and deuce reduce the recombination rate and don't disable the cell performance. [11]

To sustain electric current the injected electrons have to travel through a nanoparticle mesh to the conducting glass which is the anode of the cell. This happens via diffusion, random walking of the electron. The electron travels in the TiO_2-layer, jumping from a particle to another, eventually reaching the anode and going through a load to the cathode. At the same time triiodides go through the electrolyte towards the cathode because of the ionic diffusion. The sputtered Pt-layer which plays the role of the cathode, gives electrons to the triiodides regenerating them. These iodides delivers electrons back to the dye regenerating it. The cycle of the charge conversion is complete and the current flows through the cell [20].

1.3.2 Solid state dye device (SSDD)

A vapor phase deposition of dye should enable micro and nano devices which have been sensitized with dye. This is not possible with the current sensitation methods because PMMA masks cannot sustain multiple hours in the soaking bath containing solvents. However the fabrication is not that easy with the evaporation method either. After a sample has been fabricated with electron beam lithography (EBL) and evaporation methods, a lift off should be made to the sample. Normally this is done with acetone, which washes away the PMMA mask. The problem is that dye can't stand the acetone. Solution to this crucial trouble should be found before real nanodevices can be fabricated.

Before that, solid state dye can be used and tested with bigger, maybe micro scale, devices. One possible option is to fabricate a sandwich-type structure (Fig. 1.7). It's like a DSSC, but without electrolyte. Fabrication steps of this kind of device are basically same as they are for DSSC, except the sensitation is made with solid dye and the counter electrode is evaporated on the top of the dye layer. TiO_2 nanoparticles should be used under dye, because they provide the best adhesion and electron injection rate.

Key processes are also pretty much same as they are with DSSC, which can be seen from figure 1.8. A major difference is that electrons have to tunnel back to dye, because there is no electrolyte which provides electrons to molecules. This means that regeneration of dye shouldn't be so efficient, but there are also positive sides. Without electrolyte the possibility of recombination is even smaller, so injected electrons have higher possibility to reach an anode. This kind of devices are not designed to be solar cells, but rather sensors, which means that the bias voltage should be applied enabling the finite electric current.

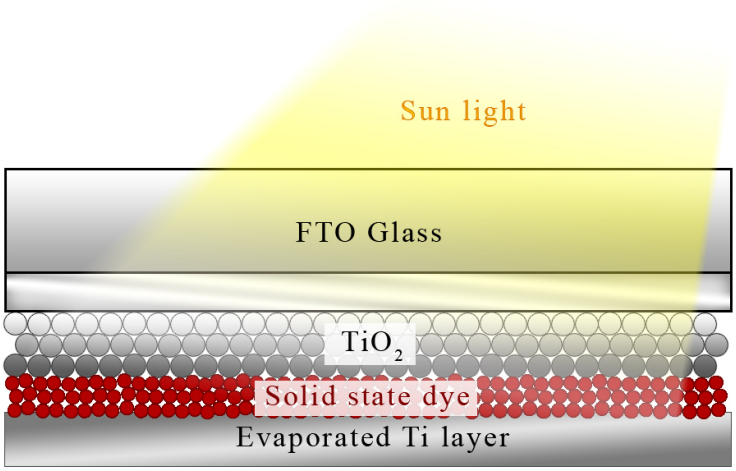

Figure 1.7: Sandwich type solid state dye device. The TiO_2 layer can be fabricated from nanoparticles or it may be grown with atomic layer deposition (ALD).

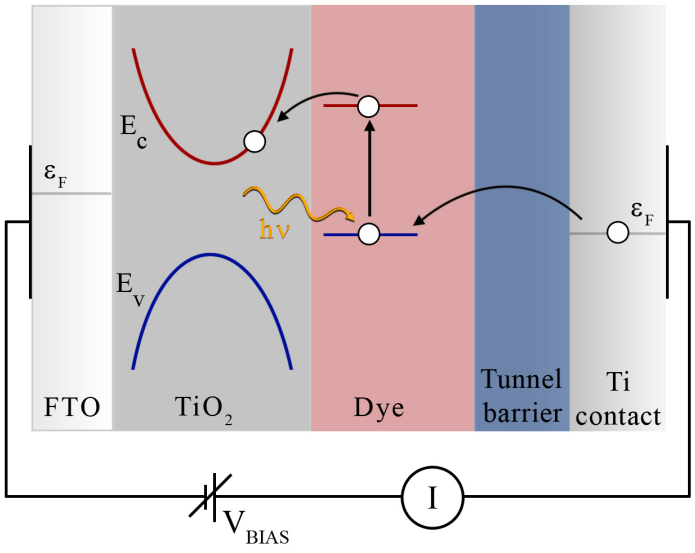

Figure 1.8: Energy diagram of a sandwich type SSDD.

A SSDD could be made also with a trapping method, where TiO_2 nanoparticle or multiple particles are trapped between the contacts by dielectrophoresis. This fabrication style has been used with carbon nanotubes [21] and DNA [22], so the method has been found to be very effective. Step towards this kind of configuration is a sample where microscale contacts made from Ti are connected with TiO_2 layer placed on top of them, as is shown in figure 1.9. After this the sample is sensitized with solid state dye. A bias voltage is used between contacts and current can be measured.

Though SSDDs are expected to be great sensors, the corresponding research work could give also new information about the dyes itself. Study of the energy spectra, properties of single dye molecule on semiconductor surface and enhanced (or reduced) photoconductivity of the sample would be the interesting topics.

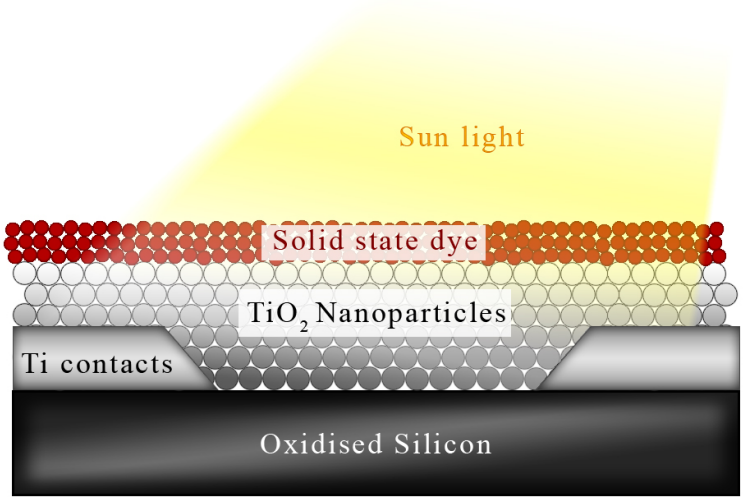

Figure 1.9: Solid state dye device made with Ti contacts.

Chapter 2

Vapour phase deposition of dye sensitizer

2.1 Why fluorescein?

We chose fluorescein for our project for several reasons. As described in previous chapter, it has been used for long time with DSSCs and has good light harvesting properties. Also its behavior with TiO_2 is well known and the method to fabricate TiO_2 layers is simple. This way sample fabrication for test samples should be easier. There was a couple of practical reasons for using fluorescein as well, especially considering the evaporation. One of the most positive things is the melting point 315 °C, which can be found in the datasheet of used fluorescein (appendix A), manufactured by *Merck Chemicals*. Because of that it can be heated securely without fear of instantly burning the molecules. One more reason was the financial one. Fluorescein is relatively cheap being a suitable material for the developing phase of the project. If something bad happens, like over heating, there are no big losses.

2.2 Evolution of the evaporator

Our evaporator underwent number of changes through out a development process. Test evaporations were performed after each change in the configuration and further developments were made grounding on this experiments. Nevertheless the basic operational principle was kept the same through the development process: a crucible is heated in a high vacuum conditions and a dye jet is guided to a sample. Method is basically same as what is used for metal evaporation.

Since the beginning the evaporator was designed having two mainparts: an evaporation chamber and a pumping unit. At first, the pumping unit was an exterior turbopump and it was attached through a tube to the side of the chamber. At this point filters were not used between the pump and the chamber. This caused some oil leakage and contamination of samples. The setup was changed when a new smaller

turbopump and an external backpump were purchased and installed. With these new pumps the evaporation chamber could be attached straight on the turbopump. This new turbopump is a dry vacuum pump so there won't be an oil contamination risk. The backpump was connected through a tube below the turbopump and an aluminum oxide filter was also installed between a pumpline and the evaporator system. Also a water cooling system and pressure gauges were added to the configuration.

The evaporation chamber is the only part which hasn't faced major changes since the first versions of the evaporator. Anyway, some of the latest and the most important upgrades have been made to it. The most vital update was the addition of a measuring crystal and electronics. The installed crystal is similar to the ones used in metal evaporators. Before that samples were placed straight on top of the hole in the cover of the evaporation pot and thickness of the evaporated dye layer was controlled by an evaporation time. With this method we knew just the relative thicknesses of evaporated layers and not absolute values. Thicknesses also varied between evaporations which could be seen from absorption spectra of the samples. Sometimes layers with smaller evaporation times gave bigger absorption maxima than layers which should have been thicker.

However the addition of the crystal brought new problems: a sample couldn't be placed right on top of the hole as the dye layer should also cover the crystal. A sample holder was made for this purpose and a couple of different formations were tested. The problem with versions lying on the pot cover (part number 7 in figure 2.2) were over heating of the crystal. This caused drifting in a evaporation rate showed by the measuring electronics. Because of these problems the sample holder was lifted and was attached to the cap of the evaporation chamber. The disadvantage of this modification was reduction in the amount of the dye deposited to the sample. To gain a better dye beam and to get a thicker layer in reasonable time, a cone was added on the hole. There is still a gradient in the horizontal profile of the beam, but this is discussed more accurately in later sections.

2.3 Current installation

The current setup of the evaporator is presented in figure 2.1. A backpump is Alcatel Pascal 2010 I and it is connected to the system trough valve number 3 and aluminium oxide filter. This prevents oil leakage to the evaporation system. The main pump is a dry turbopump Pfeiffer TMH-260 and it is attached right under the evaporation chamber as it can be seen from figure 2.2. The pumping speed of this model is 260 l/min and it reaches a pressure 10^{-6} mbar. An internal pumping system is cooled down with the cooling system where water is circulated by a waterpump manufactured by Ehein. A cooling block is in the bottom of the evaporator and it is connected to an external radiator, Zalman Tech Reserator 1.

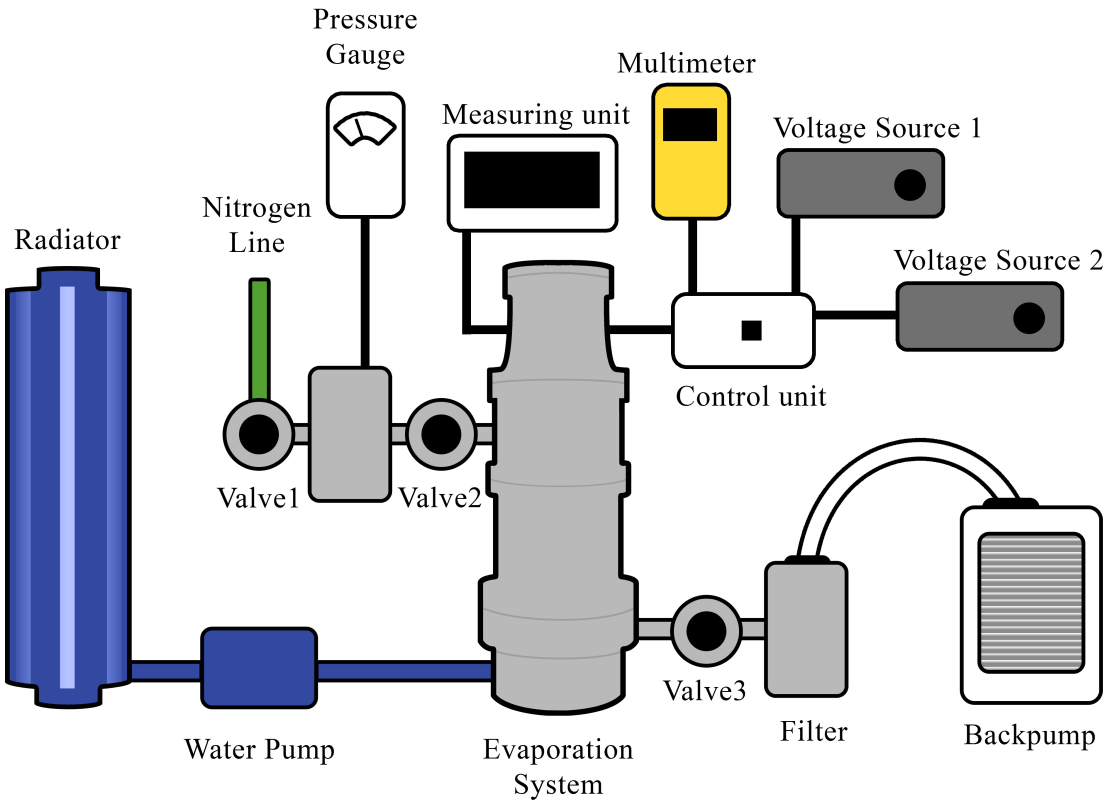

Figure 2.1: Evaporation setup.

A main part of the evaporator, the evaporation chamber, locates on the top of the system. The turbopump is separated from the chamber by a safety net. This protects the turbopump by preventing small objects, for example silicon chips, to drop into the fans. Parts of the evaporation chamber are illustrated in figure 2.2 and dimensions of the chamber are presented in appendix B. The measuring crystal is located on the sample holder which provides same dye deposition on a sample and the crystal. The deposition is monitored by the measuring unit LH Inficon Deposition monitor XTM/2, which shows a deposition rate in Å/s and the thickness of the layer in kÅ units.

Heating of the dye is made in a graphite pot. A resistor wire is coiled around the the pot and power is provided by the voltage source 1, Mascot Power supply Type 9623. This model produces maximum voltage 14.5 V, but it can be tuned down to ensure steady warming and prevent over heating. Temperature is measured with a temperature sensor which is wedged between the pot and the pot cover. Current temperature can be read from a multimeter which shows the resistance of the sensor. This can be translated to °C by a calibration curve.

Dye deposition can be controlled with a shutter. It can be operated with a button

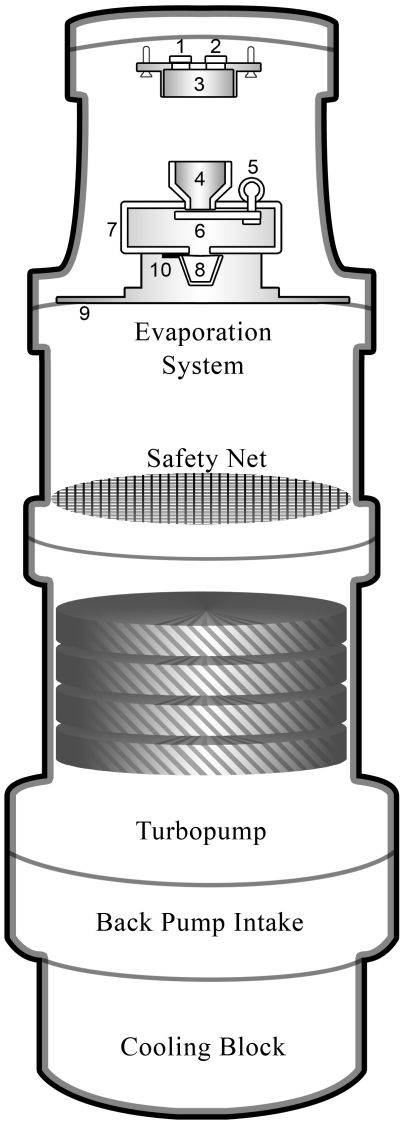

Figure 2.2: The main parts of the dye evaporator. Numbered parts of the evaporation chamber: 1 Sample, 2 Measuring crystal, 3 Sample holder, 4 Train cone, 5 Coil to move shutter, 6 Shutter, 7 Evaporation pot cover, 8 Evaporation pot; resistor wire coiled up on it, 9 Screws; holding the evaporation system, 10 Temperature sensor.

in a control unit. Both voltage sources are connected to this unit so it is an easy operation to replace one or another if needed. The shutter is getting its power from voltage source 2, HP 6259B DC Power supply. That voltage source produces 10 V which is more than enough to open and close the shutter.

There is also a sidechamber attached to the evaporator. The sensor of a pressure gauge is in this chamber. Pressure is monitored with Balzers BG 519 764-T pressure meter which unit of measure is torr. Nitrogen line is also connected to this chamber through a valve. Nitrogen is used for pressurize the evaporation chamber after a

deposition process.

2.3.1 Calibration of the temperature sensor

Used temperature sensor is a flat-film detector Pt100 manufactured by *Labfacility LTD*. Calibration points of the detector were taken from the datasheet (appendix C). Linear fitting was done to datapoints and result for parameters of the fitted line $y = A + Bx$ were $A = -275 \pm 6$ and $B = 2.72 \pm 0.03$. This graph was used when temperature was monitored by the multimeter.

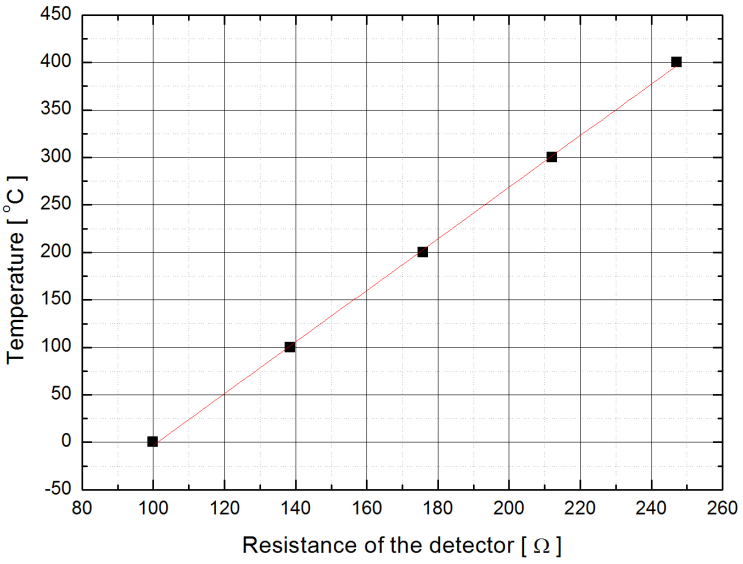

Figure 2.3: Calibration points of the detector were taken from the datasheet. Linear fitting was done to datapoints. Parameters of a fitted line $y = A + Bx$ are $A = -275 \pm 6$ and $B = 2.72 \pm 0.03$.

2.3.2 Calibration of the measuring crystal

There are two material related parameters in LH Inficon Deposition monitor XTM/2: the density of the material and Z-ratio. Neither of these parameters were known for fluorescein because these crystals are commonly used for a metal and an oxide deposition only. To simplify calibration, Z-ratio was set to 1 neglecting its contribution. The flux of the dye to a sample was found out to be relatively small and there were problems to see any positive rates by the meter. Because of that the density parameter was set to its minimum value 0.500. This makes the measuring more sensitive and atleast some value could be got with this method.

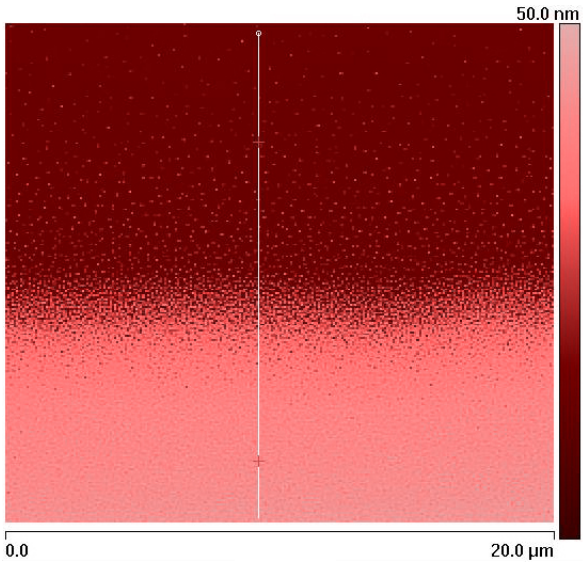

Figure 2.4: Height data of the edge of the dye square, measured with AFM. The cross-section is measured through the white line. Crosses marks the points which gives data for height difference measurement.

This method gave us just relative thicknesses of the dye layer and we didn't knew the absolute value. Calibration of the deposition monitor was made with an aid of an atomic force microscope (AFM) which gives absolute thicknesses of the layer if a clear edge could be fabricated. This caused also problems because evaporated dye used to get under the mechanical mask and made a slope very wide. Solution for this problem were a silicon chip with a nitride layer. The chip was etched to form four nitride windows which were broken. The chip was used as a mask on a silicon oxide substrate while evaporating dye layer. Four 30 µm × 30 µm dye squares were deposited. AFM images, like in figure 2.4, were taken from every side of the every square and height differences were measured with the AFM software from the cross-sections (Fig. 2.5).

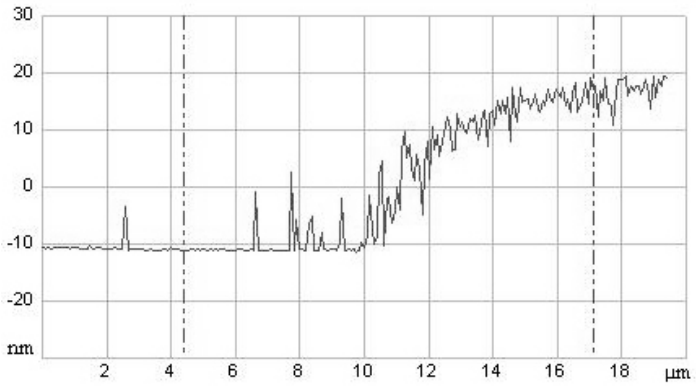

Figure 2.5: The cross-section of the dye film.

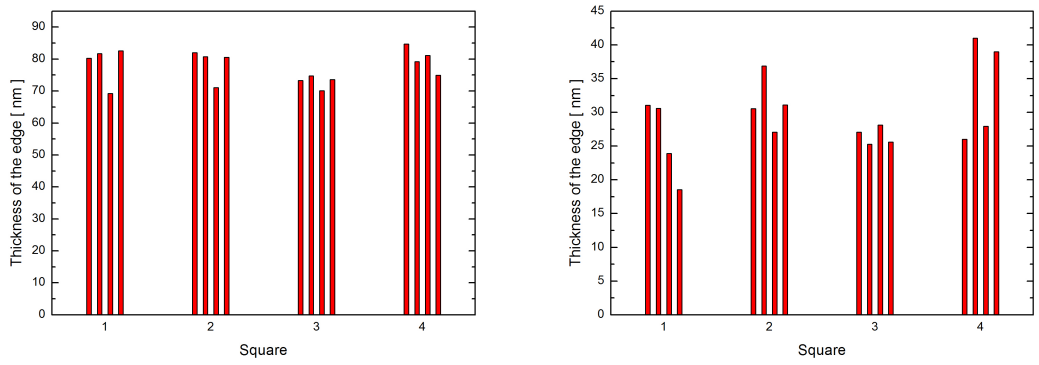

(a) (b)

Figure 2.6: Thicknesses of the dye squares deposited on oxidized silicon. Thicknesses were measured from the cross sections obtained by AFM. The mean of the values in figure (a) is 77.5 ± 1.3 nm and in (b) 29.4 ± 1.5 nm.

Measured heights are shown in figure 2.6. Mean values were calculated from this data. Like said, calibration evaporations were made with the test density parameter ρ_{test}. This means that the thicknesses read from the meter are given by

$$d_{meter} = \frac{n_{crystal}}{\rho_{test}} \cdot Z \;\Leftrightarrow\; n_{crystal} = d_{meter} \cdot \rho_{test} \cdot \frac{1}{Z}, \tag{2.1}$$

where d_{meter} is the thickness read from the meter and $n_{crystal}$ is the amount of added material measured by the crystal. Z is the Z-ratio, which is now set to 1, so it can be neglected. Of course after calibration the d_{meter} should be same as the d_{real} which is the real thickness of the layer and can be measured with the AFM. So, after calibration

$$\frac{\rho_{calib}}{n_{crystal}} = d_{calib} = d_{real} \;\Leftrightarrow\; \rho_{calib} = \frac{n_{crystal}}{d_{real}} = \frac{d_{meter}}{d_{real}} \cdot \rho_{test}. \tag{2.2}$$

Now with equation 2.2 can be calculated two values for ρ_{calib}. An error for these values can be calculated with following equation,

$$\delta\rho_{calib} = \sqrt{(\frac{1}{d_{real}} \cdot \delta d_{meter})^2 + (-\frac{d_{meter}}{d_{real}^2} \cdot \delta d_{real})^2}. \tag{2.3}$$

These equations give values $\rho_{calib1} = 0.65 \pm 0.04$ for thicker squares and $\rho_{calib2} = 1.02 \pm 0.13$ for flatter squares. So the weighted mean value $\rho_{calib} = 0.68 \pm 0.04$.

All the samples for measurements was fabricated before calibration of the meter was done. Because of that the thicknesses have to be converted afterwards. This can be done with the following equation,

$$d_{calib} = d_{meter} \cdot \frac{\rho_{test}}{\rho_{calib}} \tag{2.4}$$

and error with equation

$$\delta d_{calib} = \sqrt{(\frac{\rho_{test}}{\rho_{calib}} \cdot \delta d_{meter})^2 + (d_{meter} \cdot \frac{\rho_{test}}{\rho_{calib}^2} \cdot \delta \rho_{calib})^2}. \quad (2.5)$$

2.3.3 Evaporation process

Dye deposition in our evaporator is a four step process. First step is a loading and preparation. A sample is clamped to the sample holder and the holder is attached to the cap of the evaporator. Valve number 1 is closed and number 2 is kept open to get proper pressure reading from the gauge. After that the backpump is started and the valve number 3 is opened. Evacuation of the evaporator system closes the cap and makes it air tight. Voltage sources are turned on and the closure of the shutter is double-checked. The turbopump is started.

The next step is a pre-heating of the pot. Dye has to be heated to temperature where multimeter shows 155 Ω which is about 145 °C before deposition can be started. This takes about one to two hours. During this the rate in the crystal measuring unit is drifting between -0.1 Å/s and 0.1 Å/s and about 20 Å layer thickness is accumulated to the meter. This means that there could be some minor leakage of dye to the sample before evaporation but it is so small that it won't have a real effect.

When the necessary temperature has been reached, the shutter may be opened and the deposition meter is reset. The temperature and rate are monitored during the deposition step. Drifting of the deposition rate is usually from 0.4 Å/s to 1.2 Å/s. The pressure decreases during the deposition, but the drop is small, about $1 - 2 \cdot 10^{-5}$ torr.

After the desired layer thickness is reached the shutter is closed and the turbopump and heating are turned off. The sample and the evaporator system have to cool down at least for an hour. Meanwhile the turbopump is also running down. When the temperature has been dropped to about 50°C the system can be pressurized. The backpump is turned off and all valves are closed. The nitrogen line and the valve number 1 are turned open. This pressurizes the sidechamber. After this the valve number 2 is opened slowly to not make harm for fans of the turbopump if they are still rotating. Pressurizing also opens the cap and the sample can be removed from the evaporator.

Chapter 3

Experimental setup

3.1 Sample fabrication

The sample fabrication was performed in Nanoscience Center (NSC), Jyväskylä University. Electron beam patterning and metal deposition for samples used in electrical measurements were made in the cleanroom of NSC.

3.1.1 Samples for absorption and emission measurements

Samples for absorption and emission measurements were simple ones. They were just dye layers evaporated on different substrates. Used substrates were FTO glass, , TiO_2 nanoparticle blocks fabricated from the paste on to FTO glass and ALD (atomic layer deposition) grown 24 nm thick TiO_2 layers on glass. Transparent substrates were demanded because light must penetrate through a sample at both measurements. Reference data was measured from every substrate, so the average absorption of the substrate can be subtracted from the actual results.

TiO_2 nanoparticle blocks were fabricated with the following method. A sample substrate was masked by a tape with a hole and the nanoparticle paste Solaronix p-10 (average particle size 10 nm) was spread and leveled down with a knife blade. After that the sample was allowed to dry so that the nanoparticle block became transparent and the tape mask was removed. Next the sample was sintered in 450 °C for a half an hour to make it solid.

The properties of solid dye relating to layer thickness tried to be found out by varying the thickness of the deposited layer from 0.600 ± 0.020 kÅ to 3.000 ± 0.020 kÅ. These values were recorded from the measuring unit before calibration of the crystal was made. This way after calibration and calculating with equations 2.4 and 2.5 a scale is from 44 ± 3 to 220 ± 14 nm.

3.1.2 Samples for electric measurements

Samples for electrical measurements were fabricated using electron beam lithography (EBL) in a cleanroom environment. Oxidized silicon was used as a substrate to prevent a current flow through the substrate. At first chips were cut from the oxidized silicon wafer, size was about 1 cm $\times$ 1 cm, and were cleaned by boiling them in acetone and rinsing them in an isopropanol bath. When picked from isopropanol, chips were dried with nitrogen gas flow.

Now chips were clean and a resist layer could be spun on them. One layer resist was used because an exposed structure was simple and there were no need for angle evaporation or take account proximity effect. A4 resist was dropped on chips and they were spun with 1500 rpm speed for 60 seconds. After this chips were baked on a hot plate for 90 seconds in order to harden the resist layer. This way a 250 nm thick resist layer was accomplished.

A next step was an exposure which was performed with e-beam lithography tool LEO 1430. The exposed pattern is presented in figure 3.1. Applied exposure parameters are listed in appendix D. Two structures were drawn on a one chip with different doses in order to ensure that at least one will come out correctly. After exposure, developing was done with developer number 1: MIBK (methyl isobutyl ketone), diluted with isopropanol 1:2. The exposed patterns were developed for a minute, rinsed with isopropanol to stop developing process and dried with nitrogen flow. After this a mask was checked with an optical microscope Olympus BH2-UMA to assure that structures were opened correctly.

The mask was ready so a metal deposition can be made. This was done with Balzers Baltec BAE 250 vacuum evaporator from zero angle and the used metal was titanium. Thickness of the titanium structure was 50 nm. This thickness should be more than enough to be conductive even after natural oxidation. After metal was deposited on the sample, a lift-off was made by boiling the sample in acetone for resist removal. When an unwanted metal was stripped away the sample was washed in isopropanol and dried with nitrogen gas. A finished structure was also checked with the optical microscope.

Wires and contact pads were ready but a mask for the TiO_2 nanoparticle paste was needed. This was prepared with the PMMA also. A7 resist was dropped on the chip and the structure and it was spun with 2500 rpm for 60s to make a 500 nm thick mask. This layer was also baked for 90 seconds.

After the resist layer was finished the exposure was made. Before that the coordinates were aligned with an aid of the alignment marks (square pairs in figure 3.1). This way the nanoparticle block will be at the correct spot and cover all the wires but not the pads. This resist layer was also developed with developer number 1 just before adding the nanoparticle paste for preserving the mask.

The nanoparticle block was made with same procedure as with absorption samples,

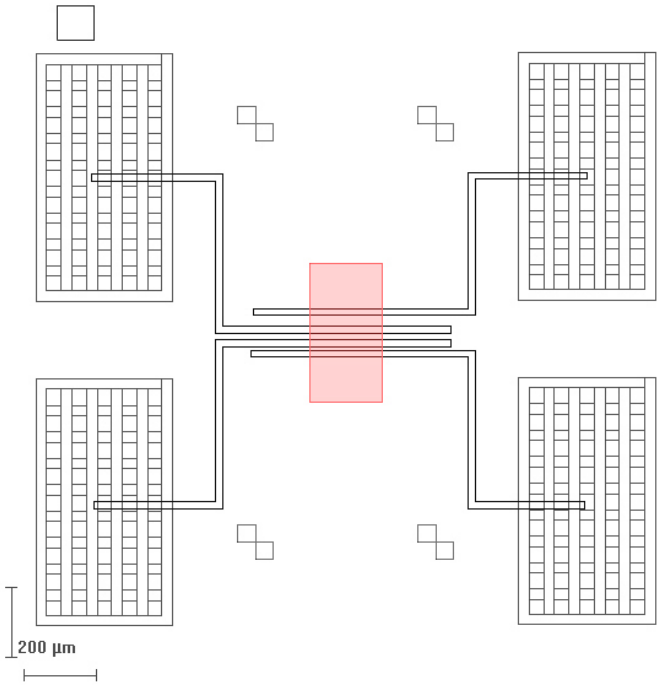

Figure 3.1: CAD-image of the exposed structure. A red square is a hole for TiO_2 particles exposed in a second step.

but the tape mask was not needed because of the PMMA mask. PMMA mask melted away during the sintering phase leaving just the nanoparticle block on the titanium wires.

3.2 Measurements

3.2.1 Absorption spectra

Absorption measurements were made with Perkin-Elmers LAMBDA 850 spectrophotometer. The measuring area of the spectrometer is just about 1 cm $\times$ 0.5 cm and because of that the sample was covered during the measurements by a paper mask with a same sized hole. This way the amount of light illuminating the sample was kept constant as well as the alignment with respect to the illumination beam area.

An absorption spectrum was measured from 400 nm to 600 nm wavelength range. Measurements were done also for just substrates (samples without dye) in order to get a reference. This way the effect of the substrate could be subtracted and the absorption spectrum of the solid dye on different substrates can be determined.

3.2.2 Emission spectra

Emission spectra were measured with Olympus Fluoview1000 confocal microscope. Measurements were done in the middle of the dye spots and on the edges. Used excitation wavelengths were 458 nm and 488 nm. Emission of the evaporated dye was measured in order to find out if the molecules had survived from the heating and were still able to work.

3.2.3 Photo-electric measurements

Electric measurements were done with the setup presented in figure 3.2. A sample was attached to a sample holder with linseed oil and the electric contact was made by wire bonding. The sample holder was contacted to BNC connectors with copper wires which were attached to a measurement block, a container made from aluminium which could be closed by cover made from conducting glass.

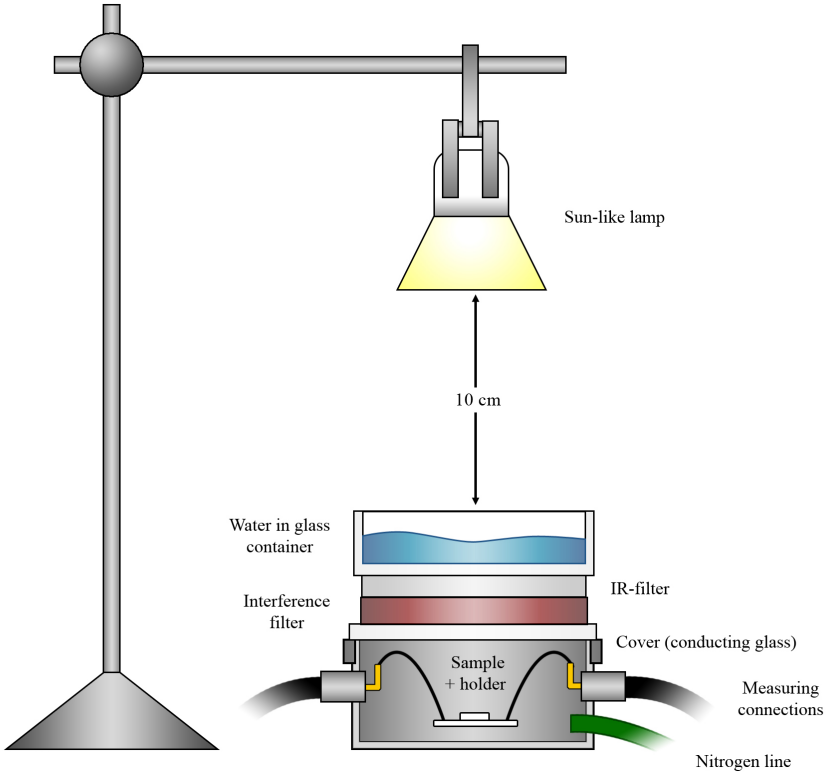

Figure 3.2: The setup of the electric measurements.

A sun like light was provided by a lamp, Q50MR16-CG-47-17, 50 Watt, 12 Volt, MR16 Halogen Spot, 4700K Bulb. During the measurements in illuminated environment, infrared radiation was filtered away with an IR- and a water filter placed on the measurement block. The sample was kept in nitrogen flow in order to eliminate large

temperature variations. Interference filters were applied to find out the wavelength dependence of the resistance over the sample.

Measurements were also done in dark. This was performed by covering the measurement block with glass cover which was painted with graphite spray paint.

AC-measurements

AC-measurements were done with the circuit presented in figure 3.3 for sandwich type structures. Fabrication of the metal contact on the sensitized nanoparticle block was found out to be impossible. Metal penetrated through the block and caused shortcuts. Because of that an electric contact was made with a graphite fiber electrode. The setup is presented in figure 3.4.

In AC-measurements current was driven through the circuit by applying a AC-voltage generated with a pulse generator. A voltage over the sample was measured. Different interference filters were used and this way wavelength dependence of the resistivity of the sample was found out.

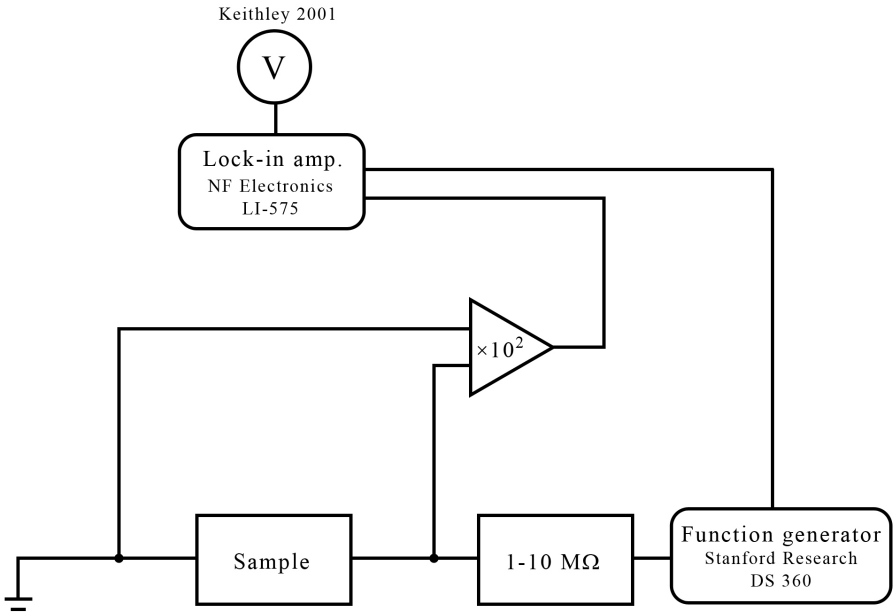

Figure 3.3: Circuit diagram of the AC-measurements in the current biased mode. Voltage was measured over the sample.

DC-measurements

DC-measurements were done with both, the sandwich type samples and the samples fabricated with EBL. Electric contacts to the samples fabricated with EBL were made

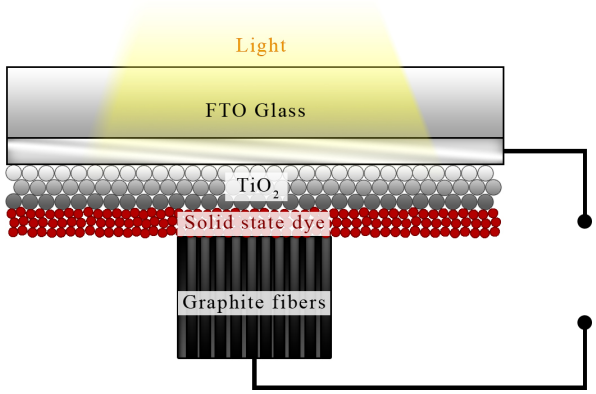

Figure 3.4: The measuring setup of the sandwich type structure, contact made with a graphite fiber electrode.

with bonding the contact pads to the sample holder with thin aluminium wires. The DC-measurement circuit is presented in figure 3.5.

An alterable source voltage was applied and this way a current was driven through the circuit. The current and the voltage over the sample were measured. A measuring time per a measuring point was kept relatively long to find out the steady state of the sample. Fast measurements didn't show the steady state of the sample because the nanoparticle samples without electrolyte had high resistivity and filling (and draining) the charge to the sample (and from the sample) was a slow process.

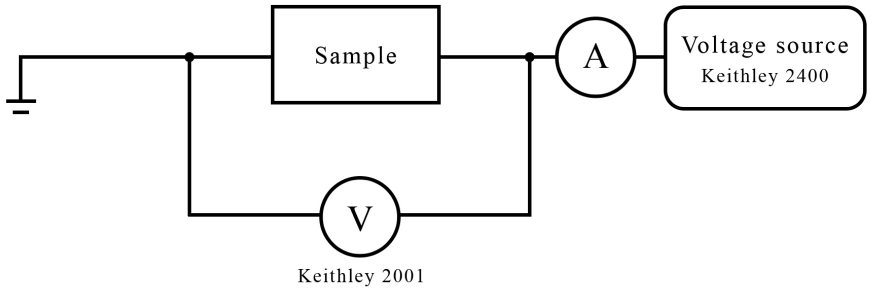

Figure 3.5: Circuit diagram of the DC-measurements. Current was driven through the sample and a voltage was measured over the sample.

Chapter 4

Results

4.1 Evaporation of fluorescein

4.1.1 Deposition rate

Typical deposition rate in our evaporation system was about 1 Å/s. If fluorescein molecules are considered as spheres which cover approximately 1.02 nm^2 [23] each, the diameter of the molecule is 1.14 nm. This means that it should take approximately 11 seconds to evaporate one monolayer.

By calculating condensation rate for our evaporator with equation 1.1, can be found out the limits of the film growth. First value is the partial pressure of the evaporated molecule gas. This is not known precisely, but it is less than or equal to measured pressure of the evaporation chamber. In the matter of fact, the pressure increase during evaporation was unnoticeable, so let's assume that the partial pressure of the dye $p = 1.0 \cdot 10^{-7}$torr $= 1.3 \cdot 10^{-5}$ Pa. Molecular mass M of fluorescein is 332.32u $= 5.52 \cdot 10^{-25}$ kg and temperature of the source was approximately 145°C which is 418 K. With these values the condensation rate of the evaporator $R = 9 \cdot 10^{16}$ $1/\text{m}^2\text{s}$.

Because the structure of the deposited dye layer is not known, let's assume ideal case where molecules are packed to hexagonal or face centered cubic lattice [24]. This means that in the quadrilateral presented in figure 4.1 there are one whole particle. The area of the quadrilateral cell is twice the area of the equilateral triangle formed by the molecule diameters,

$$A_{cell} = 2 \cdot A_{tri} = 2 \cdot \frac{\sqrt{3}\, d^2}{4} = 1.12 \cdot 10^{-18}\ \text{m}^2.$$

This way packing, it requires $8.89 \cdot 10^{17}$ particles to form a monolayer covering one square metre. If all the condensated particles absorb on the surface and fill the surface ideally, the deposition rate would be 10.6 % of the monolayer per second. Our measurements support this theory, but no further conclusions can be made without knowledge of partial pressure and additional measurements.

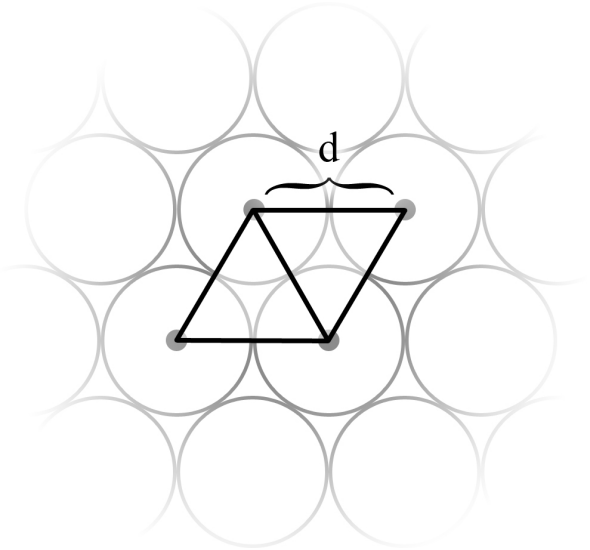

Figure 4.1: Particles packed in a hexagonal lattice.

4.1.2 Growth mode

The growth mode of the dye during the evaporation wasn't exactly investigated but AFM scans made for the calibration of the crystal revealed some interesting features. As it can be seen from figure 4.2, on the edge of the evaporated square the dye molecules are forming islands. These islands can be seen also in the cross-section image (Fig. 2.5) where they are approximately 10 nm high spikes. This could be indicating that the dye films are forming with *island growth* (Vollmer-Weber, VW) or *layer-plus-island* growth mode (Stransky-Krastanov, SK). However to determine exactly the growth mode further research should be made.

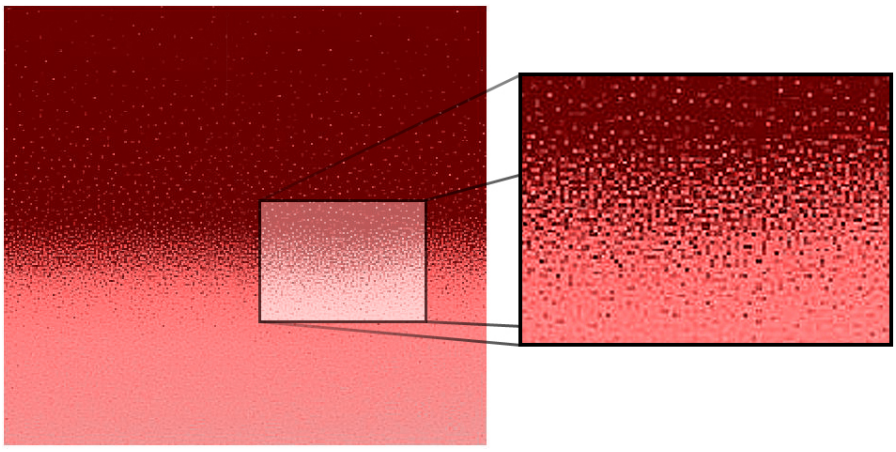

Figure 4.2: An AFM image from the edge of the evaporated dye square. Dye molecules are forming islands which can be seen from the edge area where less dye have accumulated.

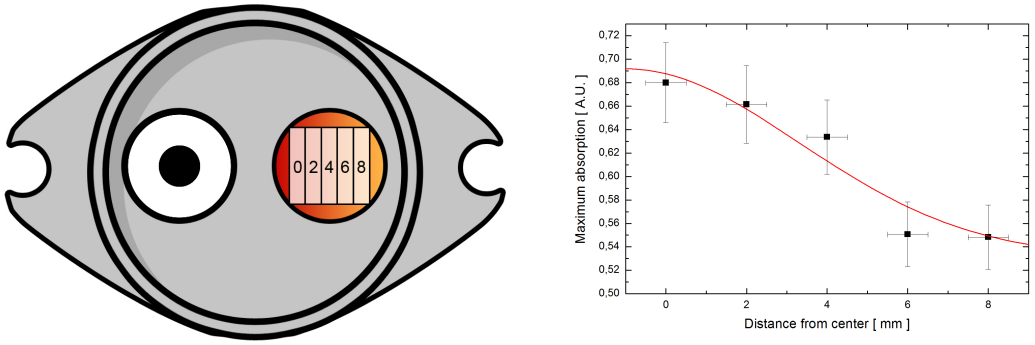

(a) (b)

Figure 4.3: (a) Measured sections of the evaporated fluorescein spot. Also placement of the crystal and a sample in sample holder is illustrated. (b) Maximum absorptions of the different sections and a fitted Gaussian curve.

4.1.3 Divergence in layer thickness

A divergence in thickness of the evaporated fluorescein layers was found out because a clear gradient could be seen even with naked eye. The variation was also measured by making a set of absorption measurements. A sample with a fluorescein layer was made with evaporator and absorptions were measured from 2 mm wide sections as presented in figure 4.3.

As it can be seen the maximum absorptions of the sections are decreasing when the distance to the center is increased. The divergence was also seen in the AFM measurements made for the calibration of the measuring crystal (Fig. 2.6), where the layer thickness varied about 10 nm in 30 µm distance.

A reason for this effect is obvious. The center maximum of the dye beam is hitting between the crystal (on the left in figure 4.3 (a)) and a sample. This is the result of the forced compromise: same amount of dye has to be deposited on a sample and on the crystal to control the overall layer thickness precisely.

4.2 Absorption spectra

4.2.1 Fluorescein dissolved to ETOH

Different amount of fluorescein were dissolved to ETOH to get a reference for solid fluorescein. Absorption spectra were measured. Measured data (scattered points) and fitted curves (continuous lines) are presented in figure 4.4. Fittings are formed from Gaussian peaks, each corresponding to a single absorption maximum:

$$y = A\ exp(-\frac{1}{2}(\frac{x - x_i}{w_i})^2)\ , (i = 1, 2, 3, 4, 5). \tag{4.1}$$

Five peaks were fitted and the parameters of the three largest ones are listed in table 4.1. Same kind of fitting were also done to some absorption spectra measured from the evaporated fluorescein layers. These results are presented later in this chapter.

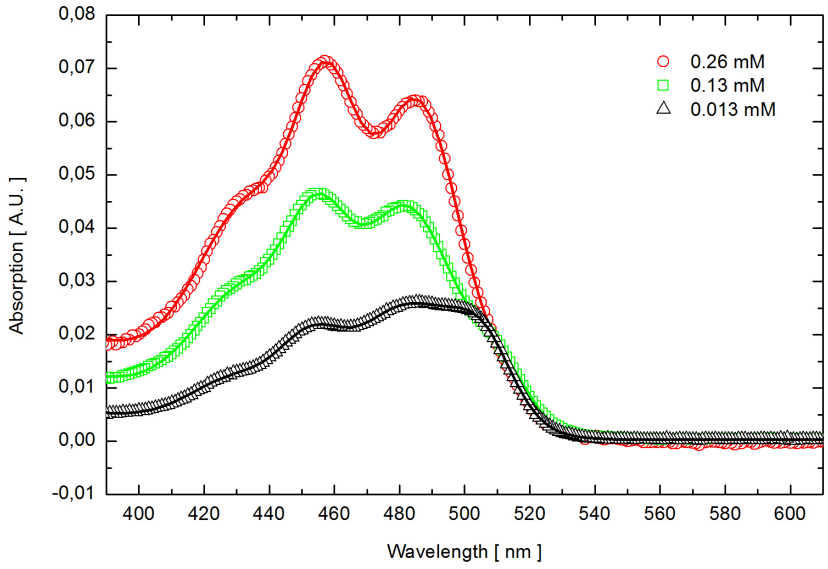

Figure 4.4: Absorption spectra of the fluorescein dissolved to ETOH with various concentrations, and fitted curves (continuous lines).

Table 4.1: The fitted maximums and their widths to absorption spectra of the dissolved fluorescein in ETOH.

Amount of fluorescein	1st max / width [nm]	2nd max / width [nm]	3rd max / width [nm]
0.013 mM	432 ± 1 / 16 ± 1	453 ± 1 / 9 ± 1	483 ± 1 / 19 ± 1
0.13 mM	434 ± 1 / 17 ± 1	455 ± 1 / 10 ± 1	482 ± 1 / 14 ± 1
0.26 mM	435 ± 1 / 17 ± 1	458 ± 1 / 10 ± 1	485 ± 1 / 13 ± 1

4.2.2 Layers evaporated before the measuring crystal

First absorption measurements were done to dye layers which were deposited on the FTO and TiO_2 nanoparticle blocks on FTO. These layers were fabricated with evaporation setup without the measuring crystal. Absorption of the substrates were subtracted

from the data. Absorption spectra of the FTO samples are presented in figure 4.5 and spectra of the nanoparticle samples in figure 4.6. Reference data of the different substrates are presented in appendix E.

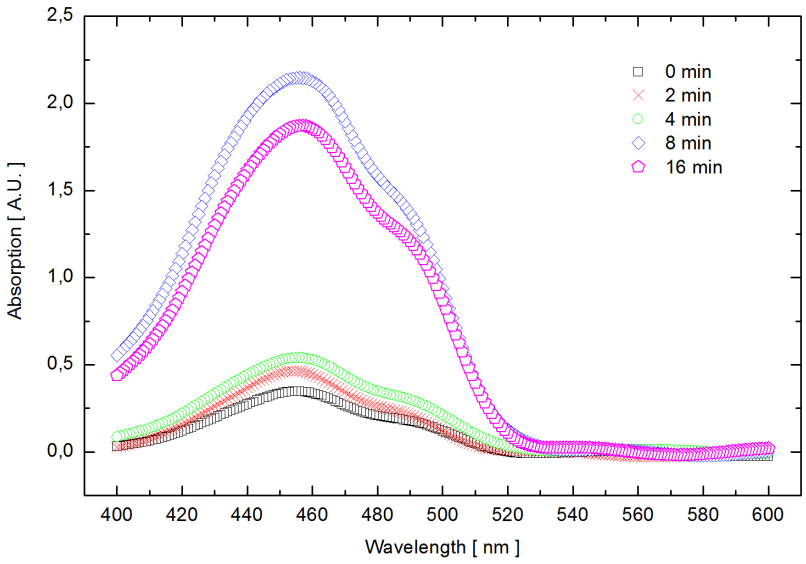

Figure 4.5: Absorption spectra of the dye layers on FTO. Thickness of the dye layer was controlled by measuring evaporation time.

As it can be seen from figures 4.5 and 4.6, controlling the dye layer thickness by evaporation time, temperature and pressure is not a accurate solution. The dye is not depositing with a constant rate and this way layer thickness may vary largely between evaporations. However on the both substrates the absorption spectra seem to have the same double peak feature in the region between 400 nm and 520 nm. This same kind of behaviour can be seen at spectra measured from dissolved fluorescein.

4.2.3 Properties of the evaporated fluorescein

The measuring crystal was added to the evaporation setup and after that the dye was deposited again on FTO. Correspondence between the measured thickness and the dye color intensity were noticed instantly even with a naked eye. This can be seen also from the absorption spectra. They are presented in figure 4.7. The figure shows clearly that the maximum absorptions of the layers follow the layer thicknesses. Dependence is close to be linear as it can be seen from figure 4.8, where the maximum absorptions are plotted as a function of the relative layer thicknesses.

After the crystal was assembled, ALD grown TiO_2 was used as a substrate. The dye gives a little bit different kind of absorption spectrum when deposited on this anatase

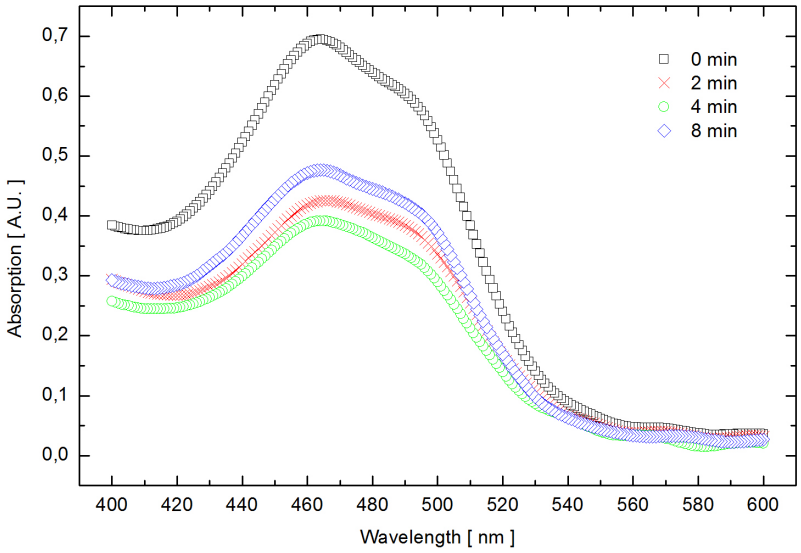

Figure 4.6: Absorption spectra of the dye layers on TiO_2 nanoparticle blocks on FTO. Thickness of the dye layer was controlled by measuring evaporation time.

base. Absorption spectra of the fluorescein on ALD grown TiO_2 and on the FTO are presented in figure 4.9. Also fitted curves are presented in figure (continuous line). Spots of the fitted maximums and their widths are listed in table 4.2.

Table 4.2: The fitted maximums and their widths to absorption spectra of the evaporated fluorescein layers on FTO and TiO_2.

Film thickness	1st max / width [nm]	2nd max / width [nm]	3rd max / width [nm]
22 ± 2 nm/ FTO	421 ± 1 / 6 ± 1	462 ± 1 / 15 ± 1	- / -
44 ± 3 nm/ FTO	428 ± 1 / 13 ± 1	454 ± 1 / 14 ± 1	484 ± 1 / 16 ± 1
66 ± 5 nm/ FTO	428 ± 1 / 10 ± 1	454 ± 1 / 19 ± 1	488 ± 1 / 14 ± 1
44 ± 3 nm/ TiO_2	427 ± 2 / 6 ± 2	468 ± 1 / 31 ± 1	500 ± 1 / 10 ± 1

When absorption spectra of the fluorescein layers on FTO are compared to the spectra measured from fluorescein in the buffer liquids (made by Sjöback, Nygren and Kubista [9]) interesting observations can be made. Spectra of the evaporated layers don't correspond straightforward to any spectra measured from different fluorescein forms in the buffer. However the spectra of the solid dye layers are close to the anion

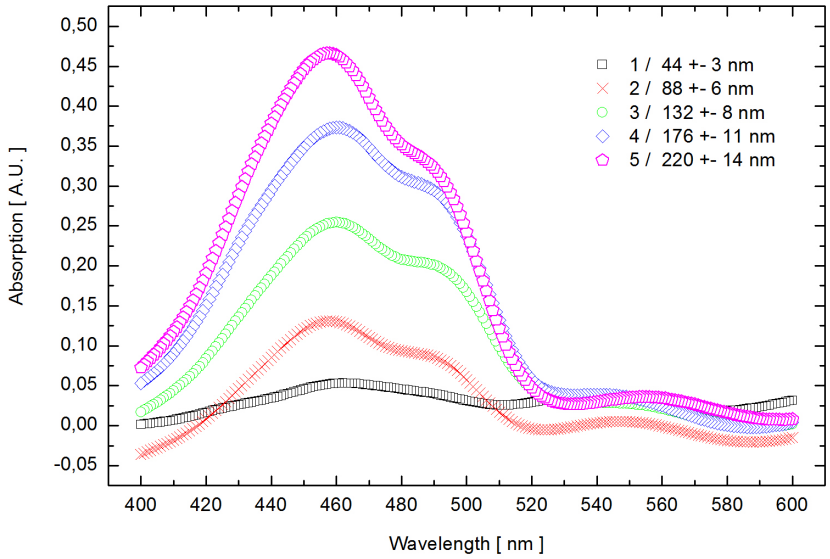

Figure 4.7: Absorption spectra of the dye layers on FTO. Thickness of the dye layers were controlled by the crystal. Absolute thicknesses were calculated after the calibration of the crystal was made.

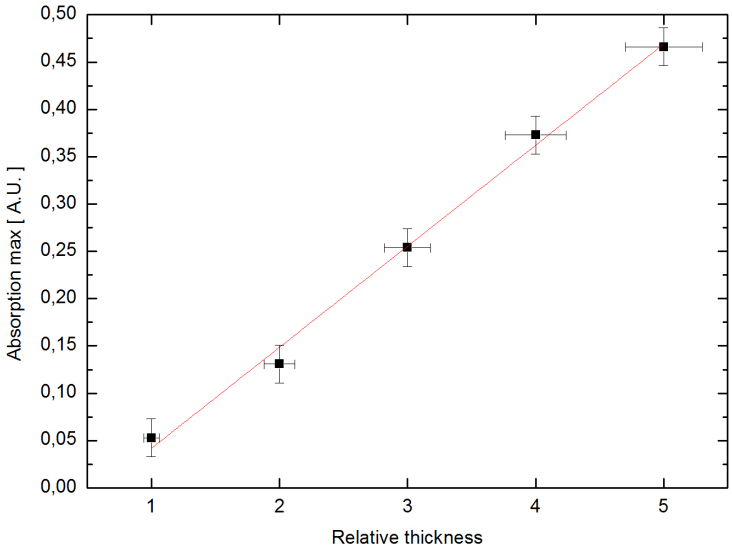

Figure 4.8: Maximum absorptions as a function of the relative thickness of the dye layer.

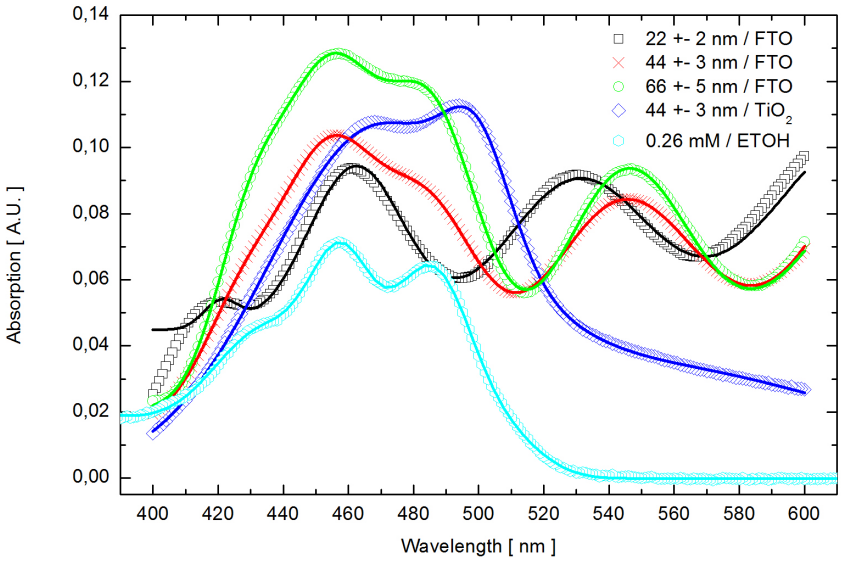

Figure 4.9: Absorption spectra of the dye layers on FTO and ALD grown TiO_2 (scattered points) and fitted curves (continuous lines). Also the spectrum of dissolved fluorescein is presented.

form spectra [9]. The overall look of the spectra and the second peak at 451 nm are similar. The third peak at 482 nm is redshifted (or blueshifted if dianion form) by 10 nm if compared to the anion in liquid. Also, it seems that making the fluorescein layer thinner redshifts the whole spectrum.

If comparison is made with our own spectra measured from fluorescein dissolved to ETOH the congruities are more obvious. The spots of the maximums are same, only the thinnest layer is making an exception. The most clear difference is magnitude of the second maximum. Where as the first maximum is dominating in the solid dye spectra, the second maximum is more distinct when fluorescein is in ETOH.

The spectrum measured from the ALD grown TiO_2 sample doesn't correspond to any spectrum measured in the buffer liquids or in ETOH. It is also redshifted by 10 nm compared to the FTO samples. This could be an effect of covalent bonding of fluorescein on the anatase TiO_2 substrate.

4.3 Emission spectra

Emission spectra were measured with two excitation wavelengths, 458 nm and 488 nm, but any significant emission couldn't be resolved with 488 nm excitation. This is interesting discovery, because usually fluorescein (in solution) gives a stronger emis-

sion at wavelengths near the excitation but the case seems to be different when solid fluorescein is excited.

4.3.1 References

Because of the dichroic filter of the excitation laser at 458 nm, peaks in shorter wavelength region are suppressed. This can be clearly seen from reference data, fluorescein dissolved to ETOH, which was measured with same system as actual samples. Emission spectrum is presented in figure 4.10 and fitting parameters (Gaussian curve, three peaks) in appendix F. There are also presented the fitted curve of the emission spectrum of fluorescein in powder form.

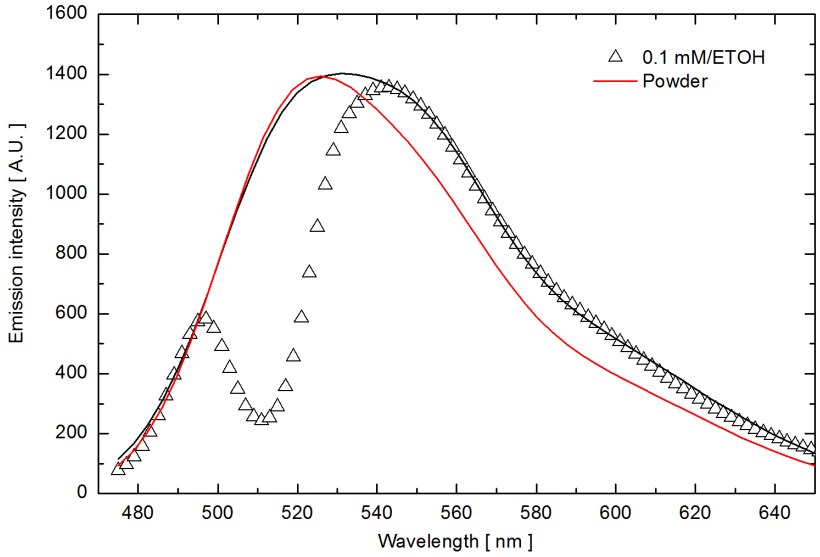

Figure 4.10: Emission spectra of the fluorescein dissolved to ETOH (scattered points) and fitted curve (continuous line). Also the fitted curve of the powder emission is presented.

4.3.2 Evaporated fluorescein on FTO glass

Gaussian curves were fitted also to emission spectra of the samples. Parameters of the fitting made for emission spectra of the fluorescein layers on FTO glass are presented in appendix F. The first maximum was estimated to be at 517 ± 5 nm (based on an estimation in figure 4.10) and it was manually set. Measured emission spectra (scattered points) and fitted curves (continuous lines) are presented in figure 4.11.

Emission spectra of solid fluorescein on FTO glass correspond to spectra of the anion and dianion forms in buffer liquid [9]. However the second maximum at 560 ±

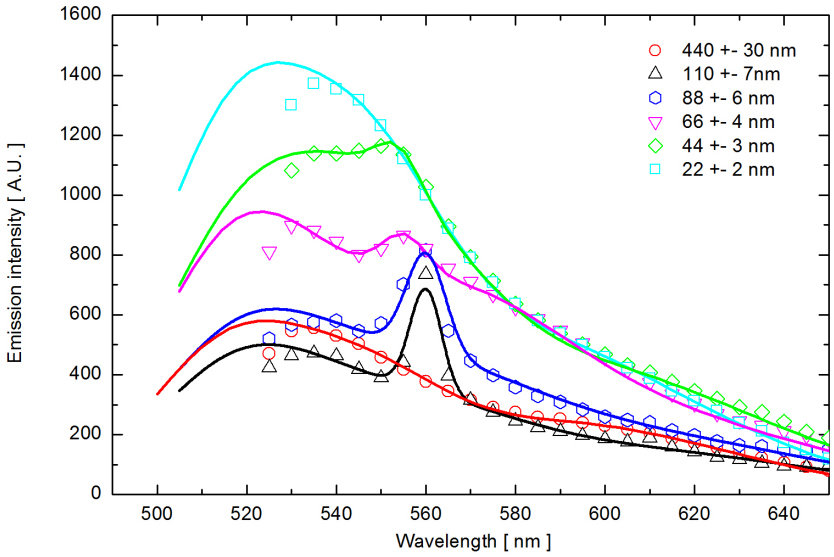

Figure 4.11: Emission spectra of the fluorescein layer deposited on FTO (scattered points) and fitted curves (continuous lines). Excitation made with 458 nm light.

5 nm is redshifting and stands out more when the layer thickness is increased. The spectra of the thin layers are similar to the spectrum of the dianion form in buffer liquid and the spectra start to remind more anion form spectra when layer thickness is increased [9]. At the same time also intensity of the emission is decreasing.

Nonetheless, emission spectra of the evaporated fluorescein layers on FTO remind very much the spectra of the references, powder and dissolved fluorescein. Only major difference is the sharp second maximum, which could be a specific feature of the ordered phase of the evaporated fluorescein.

4.3.3 Evaporated fluorescein on glass

On the glass also thinner films could be measured because the signal to noise ratio was better on smooth and thin glass than on ALD TiO_2 or FTO. The thinnest evaporated layer was 0.7 ± 1.5 nm thick, almost a monolayer, and the thickest one was 440 ± 30 nm, which can be clearly seen with a naked eye. Emission spectra were measured from these samples and Gaussian fittings were made. Fitted parameters are presented in appendix F, spectra in figure 4.12 and a close-up from the emission spectra of the two thinnest fluorescein layers in figure 4.13.

The first observation is the second maximum at 550 ± 10 nm, which appears to the spectra when the thickness of the layer is more than 0.7 nm. It seems also that maximums at 517 nm and 550 nm region are in evidence regardless of the substrate.

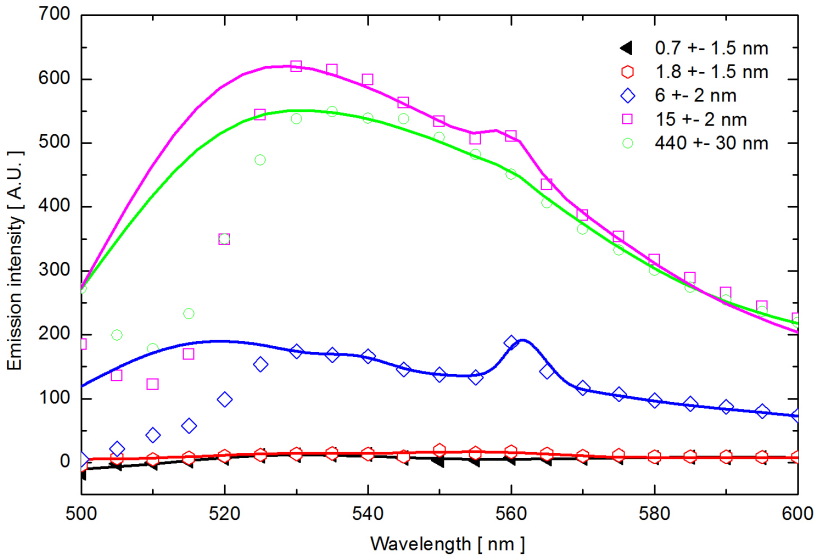

Figure 4.12: Emission spectra of the fluorescein layer deposited on glass (scattered points) and fitted curves (continuous lines). Excitation made with 458 nm light.

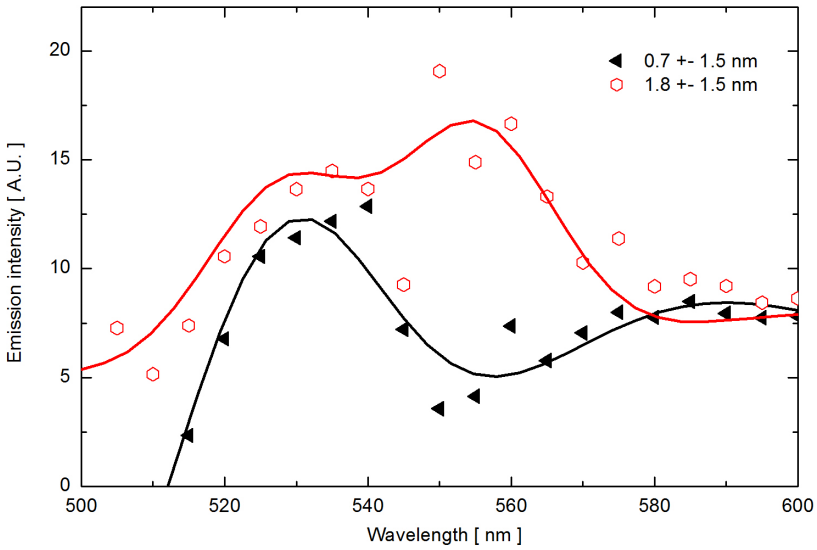

Figure 4.13: Close-up of the emission spectra of the two thinnest dye layers. Excitation made with 458 nm light.

The difference between the spectra on different substrates is the behaviour of intensities. On FTO the intensity is growing when fluorescein layer is getting thinner, but the case is totally opposite on glass. However, increasing the layer thickness from 15 nm is not affecting to the maximum intensity.

Emission spectra were measured also from the fluorescein layers deposited on ALD grown TiO_2, but emission was not observed. A probable reason for this is the electron injection to the conduction band of the semiconductor TiO_2.

4.4 Photo-electric properties

4.4.1 Wavelength dependency

Measurements of the sandwich type structure (Fig. 3.4) were made with the four-probe AC method. These measurements gave good information about the change in the resistivity of the sample under illumination and how effect is related to different wavelengths.

The voltage over the sample during the consecutive light and dark moments are presented in figures 4.14 and 4.15. The sample was illuminated with the sun-like lamp for 30 seconds and after that it was darkened for 30 seconds. As it can be seen the light has a definite effect on the sample conductivity, and it is more sensitive to some wavelengths than others.

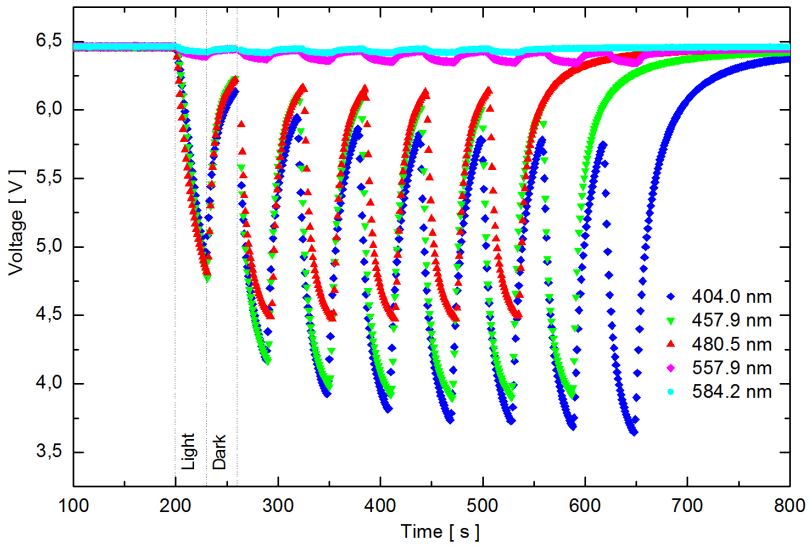

Figure 4.14: Voltage over the sample during the light and dark moments (30s each). Interference filters were used to filter the sun like lamp light.

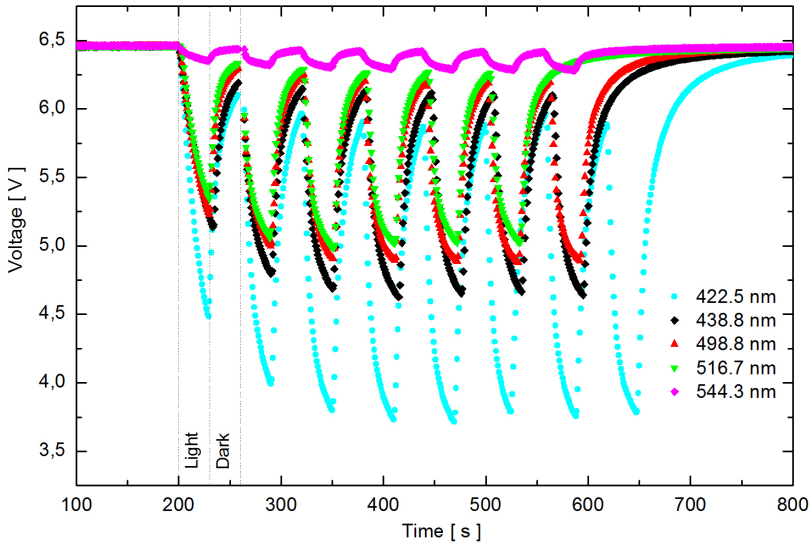

Figure 4.15: Voltage over the sample during the light and dark moments (30s each). Interference filters were used to filter the sun like lamp light.

The sample couldn't recover to the initial state during the 30 second dark sections and the voltage stayed under the initial level. However, if the sample was more sensitive to specified wavelength and this way the voltage drop was larger, also the recovering from the illumination was faster. This caused a larger voltage difference between light and dark sections when the sample was more sensitive to the tested wavelength.

The voltage minimum and maximum values were tracked from the data (the first minimum and maximum were excluded, because they deviated from the others systematically) and average difference between values were calculated for every wavelength. These voltage differences are presented in figure 4.16 where is also showed the absorption spectrum of the same kind of sample. As it can be seen the voltage difference is following the absorption. The blue end of the spectrum is causing the biggest difference to the resistivity, but the effect is getting little bit smaller until the 457 nm peak of the fluorescein. After this the effect of the light is constantly reducing when it is gone towards the red end.

4.4.2 I–V characteristics

The sandwich type sample

The sandwich type sample was measured also with DC. The voltage was swept from -7 V to 7 V and the current was monitored. Measurements were done in dark and under

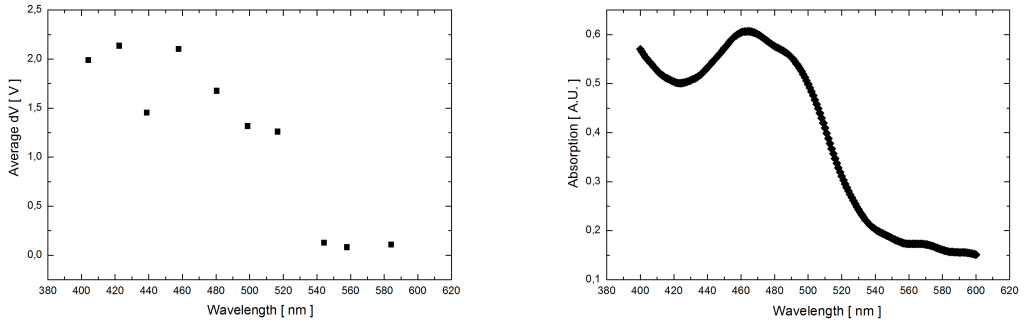

(a) (b)

Figure 4.16: The voltage minimum and maximum values were tracked from the data (the firt minimum and maximum were excluded, because they deviated from the others systematically) and average difference between values were calculated for every wavelength. (a) The average voltage difference for every measured wavelength. (b) The absorption spectrum of the same kind of sample.

illumination which was performed with led-light to reduce the effect of heating. I–V curve of the sample is presented in figure 4.17.

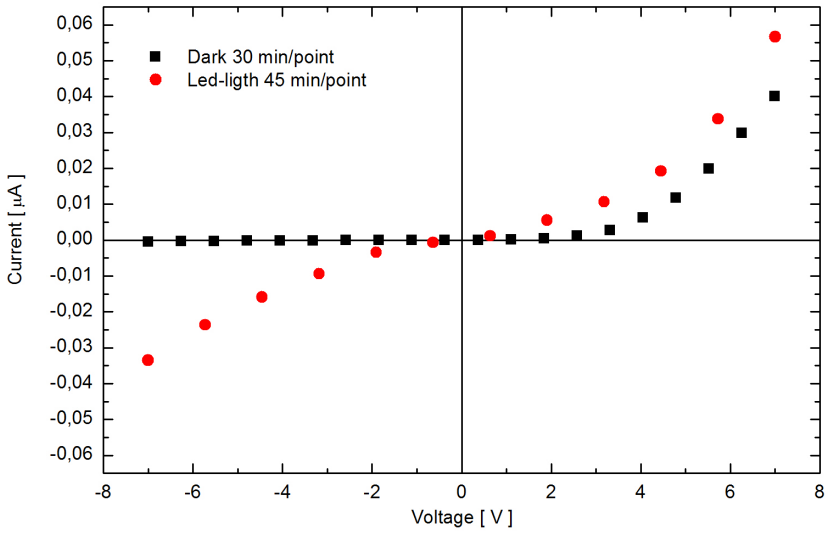

Figure 4.17: The I–V curve of the sandwich type sample measured in dark and under illumination.

The sample showed a clear diode type behaviour in dark conditions. The current is flowing through the sample only when applied voltage is positive. When the voltage

is negative the sample blocks the current totally.

When the sample is illuminated the current flows to both directions. Still the positive direction is more favourable and the current which is reached at maximum voltage is about 40% bigger in case of the positive way compared to the negative.

As it was stated in the experimental chapter the measurement time per point was relatively long. The slowness of the sample forced to this manner. This means that the effects on the sample take a long time. Building up (and draining) the charge (off) is not very efficient without an electrolyte, at least when the sample is in micrometer scale. A smaller sample could make it easier and this way provide a more effective application.

The EBL fabricated sample

When DC-measurements were done to the EBL fabricated sample (Fig. 3.1) the first observation was much larger currents than in the sandwich type structure. A clear reason for that were the dimensions. The gap between contacts were 10 µm so the resistance of the sample was of course smaller.

The I–V curve of the sample is presented in figure 4.18. The current is flowing again in both directions and the positive way is still more favourable. A new observation is a hysteresis which can be seen. Sweeping the voltage to positive side increases the resistance of the sample when the voltage is swept to opposite direction. The current reached on the negative side is smaller, until some threshold voltage is reached and the sample returns to its initial state (a close-up presented in figure 4.19). The effect is seeing more clearly when the voltage is swept more on the positive side.

The hysteresis is seen already with the -7 V to 1 V sweep, but then the effect was destroyed already under -4 V voltage. When the sample is swept to +5 V and then brought back, the effect is obvious and it takes over -6 V to destroy the effect. This causes a sudden increase in the current and this way brings the sample to its initial state.

Still the resistance of the sample is relatively high, in MΩ scale. If real applications would be liked to make, the dimensions of the sample have to be made smaller. This would decrease the resistivity and would make also the application more sensitive.

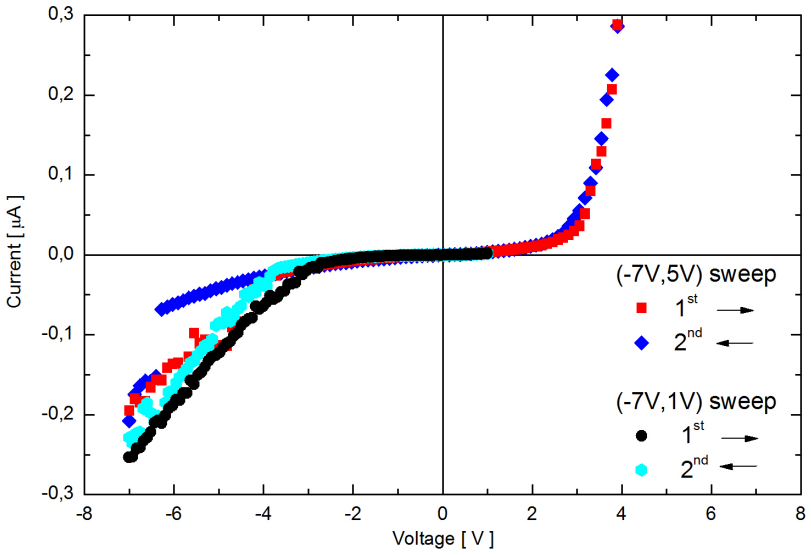

Figure 4.18: The I–V curve of the EBL fabricated sample. Measurements were done under illumination. Hysteresis can be seen when the sweep is done from -7 V to +5 V value and then came back.

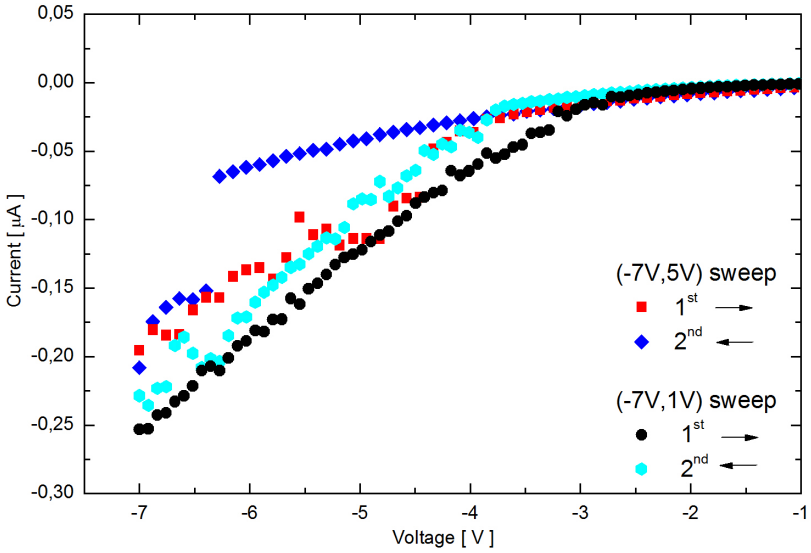

Figure 4.19: The close-up of the I–V curve of the EBL fabricated sample.

Chapter 5

Conclusions

5.1 Evaporation

Evaporation was found to be an effective and relatively easy method to sensitize different kind of substrates and samples. Heating could be made with just the resistor wire around the pot. The rate of the deposition varied so much between evaporations that it caused inconsistency to the thickness of the deposited layers. Deposited layer thicknesses couldn't be monitored just by timing, but the measuring crystal was needed for the accurate deposition rate/thickness control. This way the amount of deposited dye could be monitored during the deposition process and fluorescein layers of desired thickness could be fabricated.

There is a gradient in the horizontal axis of the dye beam during the deposition which leads to small variation in the layer thickness. This can be seen even with a naked eye. The effect of this even in the micrometer scale is insignificant, but it could be erased by developing a system to constantly moving the sample holder during the evaporation process.

5.2 Solid dye – evaporated fluorescein

Absorption measurements showed clearly that fluorescein is deposited during the evaporation. The dye also had a same kind of absorption spectrum as it have when it is dissolved in the buffer liquid or ETOH. Solid film fluorescein has it main maximum absorption peak at about 457 nm. Increasing the layer thickness also increased the maximum absorption and dependence was found to be linear.

Solid fluorescein also had good enough emission efficiency which can be measured with the confocal microscope. This proves that the deposited fluorescein has survived from the heating during the evaporation and is still active on the sample. Increasing the layer thickness didn't have so straight forward effect to the intensity as it was on the absorption. It depended on the used substrate and in the case of glass the maximum intensity saturated on layer thicknesses over 15 nm.

On the other hand, when fluorescein was deposited on ALD grown TiO_2 the emission was not seen at all. An electron injection from the dye to anatase TiO_2 semiconductor substrate could be a reason for this, giving hope to the electrical applications and measurements too.

5.3 Electrical properties

Almost all the samples were sensitive to illumination by visible light. The biggest disappointment was the failure of the sandwich type structure. The metal contact evaporated on the sensitized nanoparticle block penetrated through and caused short-cuts. Fortunately the graphite fiber contact was found out to be a useful method to measure this kind of samples.

The effect of the illumination to the samples was the drop of the resistivity. Samples conducted current much more efficiently under illumination. This effect was also found out to be wavelength depended, bigger absorption – bigger drop on the resistivity. Without dye layer, TiO_2 paste only, resistance alternation was only 1 % compared to dyed TiO_2 paste.

Measured structures also showed a diode like I–V curves under dark conditions. However, when illuminated the current flowed to the both directions, but the positive direction was still more favourable. Also a hysteresis effect was seen and it was even bigger if the voltage over the sample was swept more on the positive side. This caused the sample to block the current more efficiently when swept back until some threshold voltage destroyed the effect and brought the sample to its initial state. So, the samples showed some sort of memory related to used voltages.

Anyway, all the samples were relatively slow and measuring times had to be kept very long. The reason to this is the lack of electrolyte which would have provided electrons to the dye molecules. Fabrication of samples with smaller dimensions could be a solution to this problem.

Chapter 6

Further development & Discussion

As it has been mentioned, the main experimental problem with the solid state dye-based devices is how to decrease the dimensions. Macroscopic-size systems are working, but smaller applications would be even more sensitive. A huge obstacle is the typical EBL process, which could provide solution but dye molecules can't survive for example from the lift-off process. Some alternative solutions to this should be found out.

ALD grown TiO_2 could provide an anatase substrate where dye molecules could attach more efficiently and this way nanoparticle paste and blocks could be replaced. However, there are no needed equipments in Jyväskylä University, so this service should be bought from the outside.

Also more efficient dyes, like N3, should be tested with the evaporator. The process itself is now proved to be efficient with fluorescein, but other dyes could provide better results. Only requirement is that the used dye has some resistence to heat and doesn't burn immediately.

Bibliography

[1] R. Dole, "Use of fluorescein in the study of underground waters," *USGS Water Supply Paper*, vol. 160, pp. 73–85, 1906.

[2] M. Rezvani Khalilabad, G. Axelsson, and S. R. Gislason, "Aquifer characterization with tracer test technique; permanent CO2 sequestration into basalt, SW Iceland," *Mineral Mag*, vol. 72, no. 1, pp. 121–125, 2008.

[3] C. Jarmey-Swan, R. A. Gibbs, G. E. Ho, I. W. Bailey, and A. R. Howgrave-Graham, "A novel method for detection of viable giardia cysts in water samples," *Water Research*, vol. 34, no. 6, pp. 1948–1951, 2000.

[4] C. Blauth, J. Arnold, W. Schulenberg, A. McCartney, and K. Taylor, "Cerebral microembolism during cardiopulmonary bypass. retinal microvascular studies in vivo with fluorescein angiography," *J Thorac Cardiovasc Surg*, vol. 95, no. 4, pp. 668–676, 1988.

[5] B. O'Regan and M. Grätzel, "A low-cost, high-efficiency solar cell based on dye-sensitized colloidal TiO2 films," *Nature*, vol. 353, pp. 737–740, 1991.

[6] M. K. Nazeeruddin, S. M. Zakeeruddin, R. Humphry-Baker, S. I. Gorelsky, A. B. P. Lever, and M. Grätzel, "Synthesis, spectroscopic and a zindo study of cis- and trans-(x2)bis(4,4'-dicarboxylic acid-2,2'-bipyridine)ruthenium(ii) complexes (x=cl-, h2o, ncs-)," *Coordination Chemistry Reviews*, vol. 208, no. 1, pp. 213–225, 2000.

[7] J. Kallioinen, G. Benkö, P. Myllyperkio, L. Khriachtchev, B. Skarman, R. Wallenberg, M. Tuomikoski, J. Korppi-Tommola, V. Sundstrom, and A. P. Yartsev, "Photoinduced ultrafast dynamics of ru(dcbpy)2(ncs)2-sensitized nanocrystalline tio2 films: The influence of sample preparation and experimental conditions," *The Journal of Physical Chemistry B*, vol. 108, no. 20, pp. 6365–6373, 2004.

[8] D. Margulies, G. Melman, and A. Shanzer, "Fluorescein as a model molecular calculator with reset capability," *Nature Materials*, vol. 4, pp. 768–771, 2005.

[9] R. Sjöback, J. Nygren, and M. Kubista, "Absorption and fluorescence properties of fluorescein," *Spectrochimica Acta Part A: Molecular and Biomolecular Spectroscopy*, vol. 51, no. 6, pp. L7–L21, 1995.

[10] M. K. Nazeeruddin, A. Kay, I. Rodicio, R. Humphry-Baker, E. Mueller, P. Liska, N. Vlachopoulos, and M. Grätzel, "Conversion of light to electricity by cis-x2bis(2,2'-bipyridyl-4,4'-dicarboxylate)ruthenium(ii) charge-transfer sensitizers (x = cl-, br-, i-, cn-, and scn-) on nanocrystalline titanium dioxide electrodes," *Journal of the American Chemical Society*, vol. 115, no. 14, pp. 6382–6390, 1993.

[11] D. Cahen, G. Hodes, M. Grätzel, J. F. Guillemoles, and I. Riess, "Nature of photovoltaic action in dye-sensitized solar cells," *The Journal of Physical Chemistry B*, vol. 104, no. 9, pp. 2053–2059, 2000.

[12] G. Ashkenasy, D. Cahen, R. Cohen, A. Shanzer, and A. Vilan, "Molecular engineering of semiconductor surfaces and devices," *Accounts of Chemical Research*, vol. 35, pp. 121–128, Jan 2002.

[13] K. Sasazawa, Y. Yamada, A. Fujisawa, T. Saitoh, K. Ueno, K. Oharu, and H. Sawada, "Preparation of self-assembled fluorinated molecular aggregates, fluorescein nanocomposites: an extremely enhanced light absorption in nanocomposites," *Colloid & Polymer Science*, vol. 283, pp. 812–816, Apr 2005.

[14] V. Bulović, P. Tian, P. E. Burrows, M. R. Gokhale, S. R. Forrest, and M. E. Thompson, "A surface-emitting vacuum-deposited organic light emitting device," *Applied Physics Letters*, vol. 70, no. 22, pp. 2954–2954, 1997.

[15] J. E. Lyon, M. K. Rayan, M. M. Beerbom, and R. Schlaf, "Electronic structure of the indium tin oxide/nanocrystalline anatase (tio[sub 2])/ruthenium-dye interfaces in dye-sensitized solar cells," *Journal of Applied Physics*, vol. 104, no. 7, p. 073714, 2008.

[16] H. Lüth, *Solid Surfaces, Interfaces and Thin Films*. Berlin: Springer, 2001.

[17] T. Mizokuro, C. Heck, N. Tanigaki, T. Hiraga, and N. Tanaka, "Whitening of polymer light-emitting diodes by dispersing vapor of an orange fluorescent dye into a blue-emitting polymer film," *Applied Physics Express*, vol. 1, no. 2, p. 021804, 2008.

[18] J. Yoshinobu, K. Mukai, and T. Katayama, "A miniature effusion cell for the vacuum deposition of organic solids with low vapor pressures in surface science studies," *Review of Scientific Instruments*, vol. 79, no. 7, p. 076107, 2008.

[19] G. Benkö, M. Hilgendorff, A. P. Yartsev, and V. Sundström, "Electron injection and recombination in fluorescein 27-sensitized tio2 thin films," *The Journal of Physical Chemistry B*, vol. 105, no. 5, pp. 967–974, 2001.

[20] L. M. Peter, "Characterization and modeling of dye-sensitized solar cells," *The Journal of Physical Chemistry C*, vol. 111, no. 18, pp. 6601–6612, 2007.

[21] A. Vijayaraghavan, S. Blatt, D. Weissenberger, M. Oron-Carl, F. Hennrich, D. Gerthsen, H. Hahn, and R. Krupke, "Ultra-large-scale directed assembly of single-walled carbon nanotube devices," *Nano Letters*, vol. 7, pp. 1556–1560, May 2007.

[22] S. Tuukkanen, A. Kuzyk, J. J. Toppari, V. P. Hytönen, T. Ihalainen, and P. Törmä, "Dielectrophoresis of nanoscale double-stranded dna and humidity effects on its electrical conductivity," *Applied Physics Letters*, vol. 87, no. 18, p. 183102, 2005.

[23] H. Miyoshi, Y. Matsuo, Y. Liu, T. Sakata, and H. Mori, "Behavior of fluorescent molecules bound to the interior of silica nanocapsules in various solvents," *Journal of Colloid and Interface Science*, vol. 331, no. 2, pp. 507–513, 2009.

[24] C. Kittel, *Introduction to Solid State Physics*. New York: Wiley, 1986.

Appendices

Appendix A: Datasheet of fluorescein

The datasheet of used fluorescein was taken from the website of the manufacture.
URL: `http://www.merck-chemicals.com/fluorescein-c-i-45350/MDA_CHEM-103990/p_jBWb.s1LX0QAAAEWc9UfVhTl`
Date: 17.7.2009

103990 Fluorescein (C.I.45350)

Reag. Ph Eur

Product information

Formula Hill	$C_{20}H_{12}O_5$		
HS Code	3204 12 00	**EC number**	219-031-8
Molar mass	332.32 g/mol	**CAS number**	2321-07-5

Chemical and physical data

Melting point	314 - 316 °C	**Molar mass**	332.32 g/mol

Safety information

RTECS	LM5075000
Storage class (VCI)	10 - 13 Other liquids and solids
WGK	WGK 2 water endangering

Specifications

Assay (TBAH; calc. on dried substance)	≥ 95 %
Identity (IR-spectrum)	passes test
Melting point (DSC (differential scanning calorimetry))	about 315 °C
Absorption maximum λ max (Ethanol)	275 - 280 nm
Spec. Absorptivity A 1%/1cm (£^m^a¤; 0.02 g/l; ethanol; calc. on dried substance)	200 - 300
Loss on drying (105 °C)	≤ 5 %

Appendix B: Dimensions of the evaporation chamber

Dimensions of the evaporation chamber, unit of measure is millimeter.

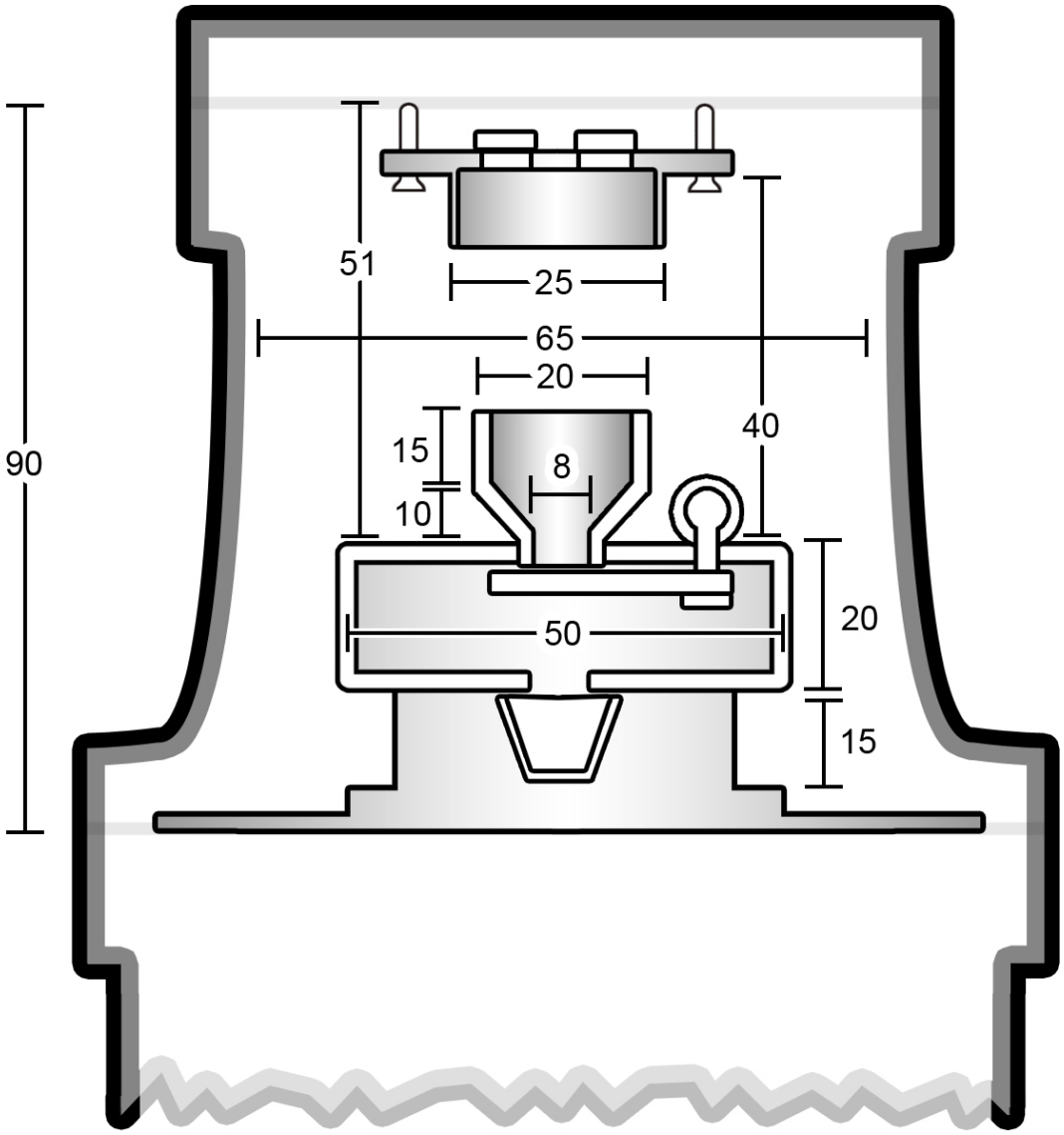

Flat-film detector Pt100 datasheet.

SPECIFICATIONS

Sensor type	Unless stated all detectors are Pt100 to BS EN60751:1996, BS1904:1984, DIN 43760:1980and IEC 751:1983
Ro	100 Ohms
Temperature range	Wire wound: -200 to +800°C
	Flat film: -50°C to maximum value shown below.

Resistance v temperature and tolerances for Pt100 thermometers to IEC 751

Temperature	Resistance	Tolerance Class A		Tolerance Class B	
(°C)	(Ω)	(±°C)	(±Ω)	(±°C)	(±Ω)
–200	18.52	0.55	0.24	1.3	0.56
–100	60.26	0.35	0.14	0.8	0.32
0	100.00	0.15	0.06	0.3	0.12
100	138.51	0.35	0.13	0.8	0.30
200	175.86	0.55	0.20	1.3	0.48
300	212.05	0.75	0.27	1.8	0.64
400	247.09	0.95	0.33	2.3	0.79
500	280.98	1.15	0.38	2.8	0.93
600	313.71	1.35	0.43	3.3	1.06
650	329.74	1.45	0.46	3.6	1.13
700	345.28	———	———	3.8	1.17
800	375.70	———	———	4.3	1.28
850	390.48	———	———	4.6	1.34

Tolerances

Class B	±(0.3°C + 0.005t)
Class A	±(0.15°C + 0.002t)

Where t is the measured temperature

1/3 Class B	±(0.1°C at 0°C)
1/5 Class B	±(0.06°C at 0°C)
1/10 Class B	±(0.03°C at 0°C)

Note: 1/3, 1/5 and 1/10 Class B Tolerances apply at 0°C

Specifications may be subject to change

Dimensions

Individual dimensions are given in Order Codes & Dimensions below.

Wire Wound

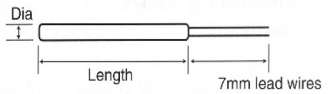

Flat-film

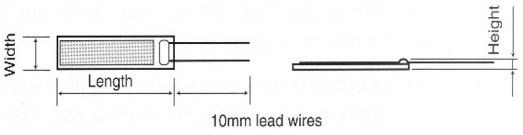

Order Codes and Dimensions

Wire Wound Detectors, PT100

Dimensions Dia x length mm)	Tolerance Class	Specification No.	Order Code
2.8 x 25	B	P100/2528 B	DA-016
2.8 x 25	A	P100/2528 A	DA-017
2.8 x 25	1/3	P100/2528 1/3	DA-018
2.8 x 25	1/5	P100/2528 1/5	DA-019
2.8 x 25	1/10	P100/2528 1/10	DA-020
1.5 x 25	B	P100/2515 B	DA-026
2.8 x 15	B	P100/1528 B	DA-041
2.8 x 15	A	P100/1528 A	DA-042
2.8 x 15	1/3	P100/1528 1/3	DA-043
2.8 x 15	1/5	P100/1528 1/5	DA-044
2.8 x 15	1/10	P100/1528 1/10	DA-045
2.4 x 15	B	P100/1524 B	DA-046
1.6 x 15	B	P100/1516 B	DA-056
1.5 x 15	B	P100/1515 B	DA-061
1.5 x 15	A	P100/1515 A	DA-062
1.5 x 15	1/3	P100/1515 1/3	DA-063
1.5 x 15	1/5	P100/1515 1/5	DA-064
1.5 x 15	1/10	P100/1515 1/10	DA-065
0.8 x 15	B	P100/0815 B	DA-081
0.8 x 15	A	P100/0815 A	DA-082
0.8 x 15	1/3	P100/0815 1/3	DA-083
0.8 x 15	1/5	P100/0815 1/5	DA-084
0.8 x 15	1/10	P100/0815 1/10	DA-085

Flat-film detectors, Pt100 and Pt1000

Sensor type	Dimensions WxLxH (mm)	Tolerance Class	Max temperature (°C)	Order Code
Pt100Ω	2 x 5 x 1.1	B	500	DM-503
Pt100Ω	2 x 5 x 1.1	A	400	DM-508
Pt100Ω	1.7 x 5 x 1.1	B	600	DM-385
Pt100Ω	2 x 10 x 1.4	B	600	DM-333
Pt100Ω	2 x 10 x 1.4	A	400	DM-334
Pt1000Ω	2 x 10 x 1.1	B	500	DM-507
Pt1000Ω	2 x 10 x 1.4	B	600	DM-367

Class A and B detectors are readily available from stock.
When ordering alternative tolerance devices please call to first to confirm availability.

For sizes and types not listed, contact sales office

Labfacility manufactures and stocks a wide range of RTD probes

LABFACILITY LIMITED

HEADQUARTERS:
LABFACILITY LTD, 8 Feltham Business Complex, Browells Lane, Feltham, Middlesex TW13 7LW Tel:+44(0)208818188 Fax +44(0)2088181881
NORTHERN DIVISION:
LABFACILITY LTD, Unit 7 Abbey Way, North Anston Trading Estate, Dinnington, Sheffield 531 7]L,UK. Tel:+44(0)1909 569446 Fax:+44(0)1909 550632
SOUTHERN and EXPORT DIVISION:
LABFACILITY LTD, Unit 7 Southern Cross Industrial Estate Shripney Road, Bognor Regis, West Sussex PO22 9SD
Tel: +44(0)1243 871280 Fax +44(0)1243 871281;

Appendix D: EBL exposure parameters

Exposure parameters used in EBL. Parameters for exposing wires and pads structure:

Structure	1	2
Coordinates	(52 ; 60)	(49 ; 60)
Spot size	510	510
Current (measured)	4.00 nA	3.90 nA
Current (set)	4.23 nA	4.00 nA
Step	8	8
Resist sensitivity	175	200

The hole for the nanoparticle paste was exposed with the parameters:

Spot size	500
Current (measured)	2.17 nA
Current (set)	2.16 nA
Step	8
Resist sensitivity	250

Reference data of the different substrates.

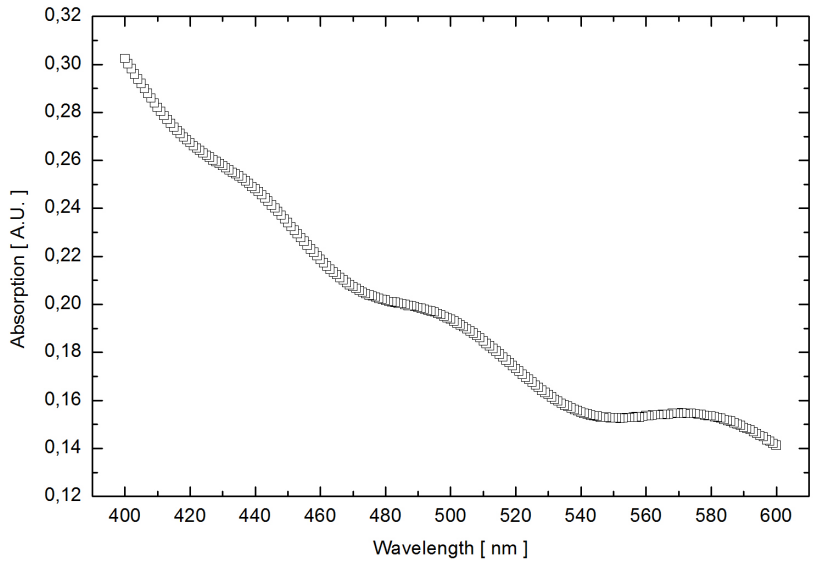

Figure E.1: Absorption spectrum of the FTO.

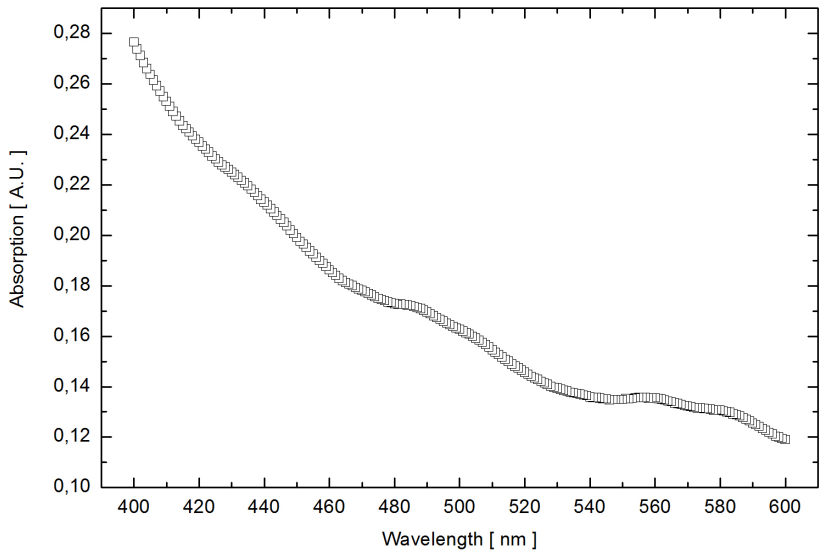

Figure E.2: Absorption spectrum of the TiO_2 nanoparticle block on FTO.

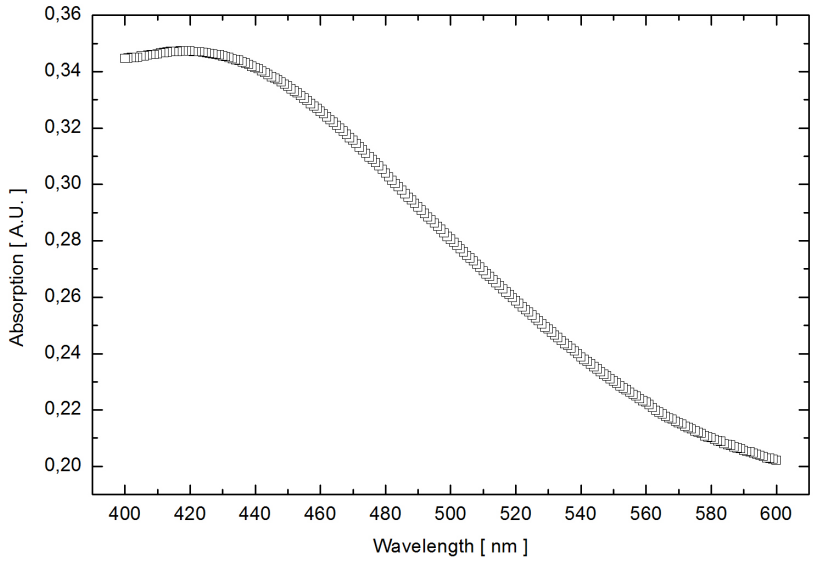

Figure E.3: Absorption spectrum of the ALD grown TiO_2 on glass.

Appendix F: Fitted parameters of the emission data

Fitted parameter for emission data (estimations) after the first maximum was forced to 517 nm.

Table F.1: Fitted maxima and their widths (estimations) to emission spectra on of fluorescein in ETOH and in powder form.

Fluorescein	1st max / width [nm]	2nd max / width [nm]	3rd max / width [nm]
0.1 mM / ETOH	517 ± 5 / 20 ± 5	550 ± 10 / 20 ± 10	580 ± 10/ 50 ± 30
Powder	517 ± 5 / 20 ± 5	549 ± 10 / 20 ± 10	580 ± 10 / 40 ± 20

Table F.2: Fitted maxima and their widths (estimations) to emission spectra on FTO glass.

Film thickness	1st max / width [nm]	2nd max / width [nm]	3rd max / width [nm]
22 ± 2 nm	517 ± 5 / 20 ± 5	548 ± 5 / 16 ± 5	574 ± 10/ 40 ± 20
44 ± 3 nm	517 ± 5 / 20 ± 5	549 ± 10 / 20 ± 10	590 ± 10 / 40 ± 20
66 ± 4 nm	517 ± 5 / 20 ± 5	560 ± 10 / 30 ± 15	600 ± 10 / 50 ± 30
88 ± 6 nm	517 ± 5 / 20 ± 5	550 ± 10 / 30 ± 15	600 ± 10 / 50 ± 30
110 ± 7 nm	517 ± 5 / 20 ± 5	560 ± 10 / 10 ± 5	600 ± 10 / 50 ± 30
440 ± 30 nm	517 ± 5 / 20 ± 5	548 ± 5 / 16 ± 5	590 ± 10 / 50 ± 30

Table F.3: Fitted maxima and their widths (estimations) to emission spectra on glass.

Film thickness	1st max / width [nm]	2nd max / width [nm]	3rd max / width [nm]
0.7 ± 1.5 nm	532 ± 2 / 20 ± 3	596 ± 4 / 80 ± 13	- / -
1.8 ± 1.5 nm	528 ± 9 / 21 ± 13	555 ± 7 / 22 ± 12	600 ± 20 / 50 ± 60
6 ± 2 nm	517 ± 5 / 20 ± 5	556 ± 5 / 15 ± 5	585 ± 5 / 30 ± 20
15 ± 2 nm	517 ± 5 / 20 ± 5	560 ± 10 / 30 ± 10	600 ± 10 / 37 ± 5
440 ± 30 nm	517 ± 5 / 20 ± 5	550 ± 10 / 30 ± 10	600 ± 10 / 32 ± 5